Biogeosciences
Discussions

Carbonyl Sulfide: Comparing a Mechanistic Representation of the Vegetation Uptake in a Land Surface Model and the Leaf Relative Uptake Approach

Fabienne Maignan[1], Camille Abadie[1], Marine Remaud[1], Linda M. J. Kooijmans[2], Kukka-Maaria Kohonen[3], Róisín Commane[4], Richard Wehr[5], J. Elliott Campbell[6], Sauveur Belviso[1], Stephen A. Montzka[7], Nina Raoult[1], Ulli Seibt[8], Yoichi P. Shiga[9], Nicolas Vuichard[1], Mary E. Whelan[10], and Philippe Peylin[1]

[1]Laboratoire des Sciences du Climat et de l'Environnement, LSCE/IPSL, CEA-CNRS-UVSQ, Université Paris-Saclay, Gif-sur-Yvette, France
[2]Meteorology and Air Quality, Wageningen University and Research, Wageningen, The Netherlands
[3]Institute for Atmospheric and Earth System Research (INAR)/Physics, Faculty of Science, University of Helsinki, Helsinki, Finland
[4]Dept. Earth & Environmental Sciences, Lamont-Doherty Earth Observatory of Columbia University, New York, NY 10964, USA
[5]Department of Ecology and Evolutionary Biology, University of Arizona, Tucson, USA
[6]Sierra Nevada Research Institute, University of California, Merced, California 95343, USA
[7]NOAA Global Monitoring Laboratory, Boulder, Colorado, USA
[8]Dept of Atmospheric & Oceanic Sciences, University of California Los Angeles, California 90095, USA
[9]Universities Space Research Association, Mountain View, CA, USA
[10]Department of Environmental Sciences, Rutgers University, New Brunswick, NJ 08901, USA

Correspondence to: Fabienne Maignan (fabienne.maignan@lsce.ipsl.fr)

Abstract. Land surface modelers need measurable proxies to constrain the quantity of carbon dioxide (CO_2) assimilated by continental plants through photosynthesis, known as Gross Primary Production (GPP). Carbonyl sulfide (COS), which is taken up by leaves through their stomates and then hydrolysed by photosynthetic enzymes, is a candidate GPP proxy. A former study with the ORCHIDEE land surface model used a fixed ratio of COS uptake to CO_2 uptake normalized to respective ambient concentrations for each vegetation type (Leaf Relative Uptake, LRU). COS leaf fluxes were then computed from GPP, and the resulting concentrations were transported with an atmospheric model which included all other known COS fluxes as inputs. Modelled COS concentrations could then be compared to COS measurements from the NOAA air sampling tower network. The LRU approach is known to have limited accuracy since the LRU ratio changes with variables such as Photosynthetically Active Radiation (PAR): while CO_2 uptake slows under low light, COS uptake is not light limited. However, the LRU approach has been popular for COS-GPP proxy studies because of its ease of application and apparent low contribution to uncertainty for regional scale applications. In this study we refined the COS-GPP relationship and implemented in ORCHIDEE a mechanistic model that describes COS uptake by continental vegetation. We compared the simulated COS fluxes against measured hourly COS fluxes at two sites, and studied the model behaviour and links with environmental drivers. We performed simulations at global scale, and estimated the global COS uptake by vegetation to be -756 Gg S yr^{-1}, in the middle range of former studies (-490 to -1335 Gg S yr^{-1}). Based on the mechanistic approach in ORCHIDEE, we derived new LRU values for the different vegetation types, ranging between 0.92 and 1.72, close to recently published averages for observed values of 1.21 for C4 and 1.68 for C3 plants. We transported the COS using the monthly vegetation COS fluxes derived from both the mechanistic and the LRU approaches, and evaluated the simulated COS concentrations at NOAA sites. Although the mechanistic approach was more appropriate when comparing to high-temporal-resolution COS flux

measurements, both approaches gave similar results when transporting with monthly COS fluxes and evaluating COS concentrations at stations. In our study, uncertainties between these two approaches are of second importance as compared to the uncertainties in the COS global budget, which are currently a limiting factor to the potential of

50   COS concentrations to constrain GPP simulated by land surface models on the global scale.

1 Introduction

Humanity has to face the urgency of climate change if it hopes to limit adverse future impacts (Allen et al., 2018; IPCC, 2019a, 2019b). In order to make reliable predictions of future climate, scientists have built powerful numerical Earth System Models (ESMs), where they continuously integrate gained knowledge on a multitude of

55   climate-related and climate-interacting processes. The carbon cycle is at the heart of the present global warming, caused by anthropogenic CO_2 emissions (Ciais et al., 2013). In the global carbon budget, the land component shows the largest uncertainty (Le Quéré et al., 2018; Bloom et al., 2016). Land Surface Models (LSMs) struggle to correctly represent the large spatial and temporal variability of the CO_2 gross and net fluxes (Anav et al., 2015). CO_2 is first assimilated through plant photosynthesis, before being respired by the ecosystem. The quantity of

60   assimilated carbon is called Gross Primary Productivity (GPP). All other carbon fluxes and stocks derive from this first gross assimilation flux. To help reduce uncertainties in the estimated GPP, LSMs can benefit from knowledge obtained through local eddy covariance measurements of the net ecosystem-atmosphere CO_2 exchange (Friend et al., 2007; Kuppel et al., 2014).

GPP proxies are also used, such as Solar-Induced Fluorescence (Norton et al., 2019; Bacour et al., 2019), isotopic

65   composition of atmospheric CO_2 ($\delta^{18}O$: Farquhar et al., 1993; Welp et al., 2011; $\delta^{13}C$: Peters et al., 2018) and Carbonyl Sulfide (COS) atmospheric concentrations (Hilton et al., 2015). Using atmospheric COS measurements as a tracer for terrestrial photosynthesis was first suggested by Sandoval-Soto et al. (2005) and Montzka et al. (2007), and Campbell et al. (2008) provided quantitative evidence using airborne observations of COS and CO_2 concentrations and an atmospheric transport model. COS is an atmospheric trace gas that has a molecular structure

70   very similar to CO_2 and is likewise taken up by plants through stomata. COS is then hydrolysed within the leaf, this reaction being catalysed by the enzyme Carbonic Anhydrase (CA). This reaction is light-independent (Protoschill-Krebs et al., 1996; Goldan et al., 1998) and, because of the high catalytic efficiency of this enzyme (Ogawa et al., 2013; Ogée et al., 2016; Protoschill-Krebs et al., 1996), COS hydrolysis inside the leaf seems therefore to be limited by COS supply driven by changes in stomatal conductance (Goldan et al., 1988; Sandoval-

75   Soto et al., 2005; Seibt et al., 2010; Stimler et al., 2010). Leaves' uptake of COS and CO_2 are thus very similar, but leaves do not produce COS (Protoschill-Krebs et al., 1996; Notni et al., 2007), whereas they emit CO_2 through respiration. That is why vegetation COS fluxes could be used as a proxy for GPP.

The approach generally adopted to constrain GPP with COS relies on the determination of a Leaf Relative Uptake (LRU), which is the ratio of COS to CO_2 uptake normalized by their atmospheric concentrations (Sandoval-Soto

80   et al., 2005):

$$LRU = \frac{F_{COS}}{GPP} \frac{[CO_2]_a}{[COS]_a} \tag{1}$$

where F_{COS} is the flux of COS uptake (µmol COS m^{-2} s^{-1}), GPP is the gross flux of CO_2 assimilation (µmol CO_2 m^{-2} s^{-1}), $[COS]_a$ is the atmospheric COS mixing ratio (µmol COS mol^{-1}), and $[CO_2]_a$ is the atmospheric CO_2 mixing ratio (µmol CO_2 mol^{-1}).

LRU can be measured experimentally, for instance in branch chambers (Kooijmans et al., 2019), and then used as

85   a scaling factor for estimating GPP. However, LRU does not appear constant under some environmental conditions. For example, the fixation of carbon from CO_2 relies on light-dependent reactions, unlike the uptake of COS by the CA enzyme, which is light-independent (Stimler et al., 2011). Because of these different responses of COS and CO_2 uptake in leaves, LRU varies with light conditions (Stimler et al., 2010, 2011; Maseyk et al., 2014; Commane et al., 2015; Wehr et al., 2017; Yang et al., 2018). Consequently, LRU values are smaller at midday or

90   in summer (Kooijmans et al., 2019). Moreover, COS assimilation continues at night as stomatal conductance to gas transfer does not drop to zero, whereas CO_2 uptake by plants stops, leading to an infinite value of LRU. Note however that stomata mostly close at night, so the COS uptake at night is smaller than the COS uptake during the day. It has also been shown that LRU varies between plant species (Stimler et al. 2011), which is why different LRU values were estimated for different vegetation types (Seibt et al., 2010; Whelan et al., 2018). The variability

95   of LRU with plant type, light, and time should therefore be carefully accounted for when COS concentrations or flux measurements are used to estimate GPP at the ecosystem and larger scales.

The goal of this study is thus to evaluate the advantages of using a mechanistic approach to simulate the uptake of atmospheric COS by continental vegetation within a Land Surface Model (LSM), as compared to the former LRU approach developed in Launois et al. (2015b), where the authors simply defined the COS uptake by vegetation as

100   that of CO_2 scaled with a constant LRU value for each large vegetation class. To this end:

i)   We used the state-of-the art ORCHIDEE LSM (Krinner et al., 2015), and implemented in it the vegetation COS uptake model of Berry et al. (2013) to simulate the COS fluxes absorbed at the leaf and canopy levels by the continental vegetation.

ii)   We evaluated the simulated COS fluxes against measurements at two forest sites, namely the Harvard

105   Forest, United States (Wehr et al., 2017), and Hyytiälä, Finland (Kooijmans et al., 2019; Kohonen et al., 2020; Sun et al., 2018a).

iii)   We compared the simulated mechanistic COS fluxes at global scale to former estimates and also compared different estimates of LRU values.

iv)   The mechanistic and LRU simulated COS fluxes were used with the atmospheric transport model LMDz

110   (Hourdin et al. 2006), to provide atmospheric COS concentrations that were evaluated against measurements at sites of the NOAA network.

We present the model, data, and methodologies related to these four steps in section 2, detail the obtained results in section 3, and discuss them in section 4. We conclude and list paths for future research in section 5.

2 Models, Data, and Methodology

115   ### 2.1 Implementation of plant COS uptake in the ORCHIDEE LSM to simulate COS vegetation fluxes

2.1.1 The ORCHIDEE LSM

ORCHIDEE is an LSM developed mainly at Institut Pierre Simon Laplace (IPSL), that computes the water, carbon and energy balances at the interface between land surfaces and atmosphere. Fast processes including hydrology, photosynthesis and energy balance are run at a half-hourly timestep, while other slower processes such as carbon

120   allocation and mortality are simulated at a daily timestep. Photosynthesis follows the Yin and Struik (2009)

approach, bringing improvements to the standard Farquhar et al. (1980) model for C3 plants, the Collatz et al. (1992) model for C4 plants, and the Ball et al. (1987) model for the stomatal conductance. The temperature-dependence of the photosynthetic capacity follows the Kattge and Knorr (2007) model. A water stress function varying between 0 and 1 depending on soil moisture and root profile (de Rosnay and Polcher, 1998) is applied on

125 photosynthetic capacity and conductances. The sub-grid variability for vegetation is represented using fractions of Plant Functional Types (PFTs), grouping plants with similar morphologies and behaviours growing under similar climatic conditions. Phenology is fully prognostic with PFT-specific phenological models as described in Botta et al. (2000) and MacBean et al. (2015). ORCHIDEE can be run from the site scale to the global scale, coupled with an atmospheric general circulation model, or in off-line mode forced by meteorological fields. In this study, we

130 prescribed the vegetation distribution for site simulations and used yearly PFT maps derived from the ESA Climate Change Initiative (CCI) land cover products for global simulations (Poulter et al., 2015). The soil type is derived from the Zobler map (Zobler, 1986). We used the recent ORCHIDEE version fine-tuned for the Climate Model Intercomparison Project (CMIP) 6 exercise (Peylin et al., *in prep*.), forced by micro-meteorology fields at FLUXNET sites or by CRUNCEP reanalyses at global scale (https://rda.ucar.edu/datasets/ds314.3/).

135 **2.1.2 The Berry model for plant COS uptake**

We implemented in the ORCHIDEE LSM the mechanistic model of plant COS uptake based on Berry et al. (2013). In this model, COS follows a diffusive law from the atmosphere to the leaf interior, where it is consumed by CA in the chloroplasts. The uptake from the atmosphere is assumed unidirectional, reflecting the fact that COS is not produced by plants. The model distinguishes three conductances along the COS path between the atmosphere and

140 the leaf interior: (1) the boundary layer conductance (g_{B_COS}) to heat and gas transfer between the leaf surface and the atmosphere, (2) the stomatal conductance (g_{S_COS}), and (3) the internal conductance (g_{I_COS}). Internal conductance combines the mesophyll conductance and the CA activity into a single equivalent conductance. The stomatal and boundary layer conductances are associated with factors describing diffusion of COS relative to that of water vapor (1.94 and 1.56, respectively, Stimler et al., 2010). In the chloroplast, the COS hydrolysis is

145 catalysed by the enzyme CA, following first order kinetics. COS uptake depends on the amount of CA and its relative location to intercellular air spaces, which brings in the mesophyll conductance. These two factors have been shown to scale with the maximum reaction rate of the Rubisco enzyme, V_{max} (µmol m^{-2} s^{-1}) (Badger and Price, 1994; Evans et al., 1994). The mesophyll conductance and the first-rate constant are then regrouped into a single equivalent internal conductance, proportional to V_{max}:

$$g_{I\_COS} = \alpha * V_{max} \qquad (2)$$

150 The parameter α takes two values depending on the plant photosynthetic pathway (C3 or C4). These values were determined experimentally by Berry et al. (2013), who estimated an $\alpha = 0.0012$ for C3 and an $\alpha = 0.013$ for C4 species. We thus have the final equation:

$$F_{COS} = [COS]_a * \left[\frac{1.0}{g_{S\_cos}} + \frac{1.0}{g_{B\_cos}} + \frac{1.0}{g_{I\_cos}}\right]^{-1} = [COS]_a * \left[\frac{1.94}{g_{S\_W}} + \frac{1.56}{g_{B\_W}} + \frac{1.0}{g_{I\_cos}}\right]^{-1} \qquad (3)$$

where F_{COS} is the flux of COS uptake (µmol COS m^{-2} s^{-1}), $[COS]_a$ is the background atmospheric COS mixing ratio considered here as a constant (0.0005 µmol COS mol^{-1}), g_{S_cos}, g_{B_cos} and g_{I_cos} are respectively the

155 stomatal, boundary layer, and internal conductances to COS (mol COS m^{-2} s^{-1}), and g_{S_W} and g_{B_W} are respectively the stomatal and boundary layer conductances to water vapor (mol H$_2$O m^{-2} s^{-1}). Note that in this work

$[COS]_a$ is held constant when computing the COS fluxes, contrary to Berry et al. (2013) and Campbell et al. (2017), where $[COS]_a$ is dynamic and taken from the previous time step's PCTM (Parameterized Chemical Transport Model) value. The uncertainty introduced by this simplification is evaluated in the Discussion section.

2.1.3 Minimal conductances

As plant CO_2 uptake only occurs under certain conditions such as with sufficient light, temperature, and water, CO_2 assimilation is not calculated in ORCHIDEE when these conditions are not fulfilled. Therefore, the stomatal conductance to CO_2 that is needed to obtain the stomatal conductance to COS is not always computed in ORCHIDEE. However, some studies have shown incomplete stomatal closure at night (Lombardozzi et al., 2017; Kooijmans et al., 2019), leading to nighttime COS plant uptake (Berry et al., 2013; Kooijmans et al., 2017). Therefore, we had to define a minimal stomatal conductance to COS under these particular conditions when there is no CO_2 assimilation. The minimal conductance to CO_2 used in ORCHIDEE is based on the residual stomatal conductance if the irradiance approaches zero, represented as the g_0 offset in the stomatal conductance models (see equations (15) for C3 and (25) for C4 plants in Yin and and Struik, 2009). In the absence of water stress, g_0 takes a constant value for C3 (0.00625 mol CO_2 m^{-2} s^{-1}) and C4 (0.01875 mol CO_2 m^{-2} s^{-1}) plants. This constant is multiplied by a water-stress function to compute the minimal conductance. This minimal conductance to CO_2 was then applied under conditions when there is no CO_2 assimilation, multiplied by the ratio to convert the conductance to CO_2 into a conductance to COS. We thus model COS assimilation even at night, for all PFTs, and in winter for evergreen species, depending on water stress conditions.

2.1.4 Simulations protocol

All simulations were preceded by a "spin-up" phase to get to an equilibrium state where the considered carbon pools and fluxes are stable with no residual trends in the absence of any disturbances (climate, land use change, CO_2 atmospheric concentrations) (e.g. Wei et al., 2014). A few decades are enough to equilibrate above-ground biomass and GPP. As we will transport not only COS, but also CO_2 (see Sect. 2.4 below), we need a longer spin-up where all carbon pools including those in the soil are stable and the net CO_2 fluxes oscillate around zero. Equilibrating the ecosystem photosynthesis with its respiration takes a long time as the slowest soil carbon pool has a residence time on the order of one thousand years. The ORCHIDEE model has a built-in spin-up procedure to accelerate the convergence towards this equilibrium state, using a pseudo-analytical iterative estimation of the targeted carbon pools, based on Lardy et al. (2011). For global simulations, we first performed a 340-year spin-up phase with non-varying pre-industrial atmospheric CO_2 concentration and vegetation map, cycling over the same 10 years of meteorological forcing files, where the final relative variation of the global slowest soil carbon pool was less than 5%. Starting from this equilibrium state, a transient state simulation was then run applying climate change, land use change and increasing CO_2 atmospheric concentrations, and COS and GPP fluxes were calculated from 1860 to 2017. We performed site simulations at the Harvard Forest (United States) and Hyytiälä (Finland) FLUXNET sites (see below). For the two sites, we first performed a spin-up simulation cycling over the available years of the FLUXNET forcing files, for around 340 years, using a constant atmospheric CO_2 concentration corresponding to the first year of the FLUXNET forcing file. We then performed the transient simulations over the available FLUXNET years, for each site, with a varying CO_2 atmospheric concentration.

2.2 Evaluation of vegetation COS fluxes at two FLUXNET sites

195   Vegetation COS flux direct or derived measurements were available at the Hyytiälä (Finland) and Harvard Forest (United States) FLUXNET sites. The Hyytiälä site (61.85°N, 24.29°E) is a boreal evergreen needleleaf forest dominated by Scots pine. Branch measurements of COS fluxes were made in a Scots pine tree from March to July 2017 using gas-exchange chambers (Kooijmans et al., 2019); fluxes were derived from mole fraction changes when the chambers were closed once every hour. Measurements were made with an Aerodyne Quantum Cascade

200   Laser Spectrometer (QCLS) and were calibrated against reference standards (Kooijmans et al., 2016). Fluxes from empty chambers were regularly measured to be able to correct for gas exchange by the chamber and tubing material (Kooijmans et al., 2019). We also used the Hyytiälä COS ecosystem fluxes (Kohonen et al., 2020); eddy covariance fluxes were measured during years 2013-2017 at 23 m height, approximately 6 m above the canopy height. Flux data were processed, quality screened and gap-filled according to recommendations by Kohonen et al. (2020).

205   Soil fluxes were also available for year 2015 (Sun et al., 2018a), we thus derived the COS vegetation fluxes at canopy scale for that year from the difference between ecosystem and soil fluxes. Soil fluxes were generally low compared to plant uptake.

The Harvard Forest site (42.54°N, 72.17°W) is a temperate deciduous broadleaf forest with mainly red oak, red maple and hemlock. Ecosystem COS eddy flux measurements were carried out from a tower from May to October,

210   in 2012 and 2013, using an Aerodyne QCLS and calibrated using gas cylinders. They were further split into vegetation and soil components, using soil chamber CO_2 measurements and a sub-canopy flux-gradient approach (Wehr et al., 2017).

The simulated COS fluxes were evaluated against measurements using the Root Mean Square Deviation:

$$RMSD = \sqrt{\frac{\sum_{n=1}^{N}\left(F_{COS}^{Obs}(n) - F_{COS}^{Mod}(n)\right)^2}{N}} \qquad (4)$$

where N is the number of considered observations, $F_{COS}^{Obs}(n)$ is the nth observed COS flux and $F_{COS}^{Mod}(n)$ is the nth

215   modelled COS flux, and the relative RMSD:

$$rRMSD = \frac{RMSD}{\frac{\sum_{n=1}^{N} F_{COS}^{Obs}(n)}{N}} \qquad (5)$$

which is the RMSD divided by the mean value of observations.

2.3 Global scale flux estimates and Comparisons with the LRU approach

We compared our estimate for plant COS uptake at global scale to former studies, with a focus on the LRU approach, evidencing some uncertainties when possible. We also applied the LRU approach to derive new

220   estimates of global plant COS uptake for comparison, using a monthly climatology of our modelled GPP fluxes over the 2000-2009 period, a constant atmospheric concentration of 500 ppt for COS and global yearly values for CO_2 (from 368 ppm for year 2000 to 386 ppm for year 2009). We considered two sets of constant PFT-dependent LRU values. The first set (LRU_Seibt) was taken from Seibt et al. (2010), based on the observed LRU values displayed in their Table 3 (intermediate column). The second set (LRU_Whelan) used constant values for C3

225   (1.68) and C4 (1.21) plants where the values are an average over different field and laboratory measurements as assembled by Whelan et al. (2018). Both sets are listed in Table 6.

Reciprocally, we derived LRU values using the monthly climatology of our modelled COS and GPP fluxes over the 2000-2009 period. LRU values were computed for all strictly positive GPP values. For each PFT, we studied

the spatio-temporal distribution of LRU values among grid cells where the PFT was present. Considering that the objective of the LRU approach was to estimate COS fluxes from GPP using a constant value per PFT, the optimal LRU value for each PFT was obtained by linearly regressing COS fluxes against GPP multiplied by the ratio of the mean COS to CO_2 concentrations, with no offset, thus:

$$LRU\_Opt = \frac{\sum_{n=1}^{N} F_{COS}^{Mod}(n) GPP^{Mod}(n) \frac{[COS(n)]_a}{[CO_2(n)]_a}}{\sum_{n=1}^{N} \left(F_{COS}^{Mod}(n) \right)^2} \quad (6)$$

with N the number of grid cell-month simulated fluxes where the PFT is present in the monthly climatology.

We compared this new set of optimal PFT-dependent LRU values against LRU_Seibt and LRU_Whelan.

We finally used the LRU_Opt values to re-compute the monthly mean COS fluxes from our modelled monthly mean GPP, and compared with the mechanistic COS flux calculation. The differences, due to the non-linearity of the COS flux calculation, provide some information on the use of a simplified approach based on mean LRU values.

2.4 Simulations of COS concentrations and Evaluation at NOAA air sampling sites

The vegetation COS fluxes, as well as all other sources and sinks of the global COS budget, based on their latest estimates, are transported with an atmospheric transport model, so that we are able to simulate 3D COS atmospheric concentrations and compare them to the NOAA surface measurements.

2.4.1 The atmospheric transport model LMDz

In order to simulate COS and CO_2 concentrations in the atmosphere, we used the version of the atmospheric component LMDz of the Institut Pierre-Simon Laplace Coupled Model (IPSL-CM) (Dufresne et al., 2013) which has been contributing to the CMIP6 exercise. To reduce the computation time, we used its off-line mode: precomputed air mass fluxes provided by the full version of LMDz are used to transport the different tracers (Hourdin et al., 2006). This version is further called LMDz6 and is described in Remaud et al. (2018) and references therein for the transport of CO_2. The horizontal winds are nudged towards ECMWF meteorological analyses (ERA-5, https://www.ecmwf.int/en/forecasts/datasets/archive-datasets/reanalysis-datasets/era5) to realistically account for large scale advection. The tropospheric OH oxidation of COS is calculated from OH monthly data that are produced from a first simulation done with the INCA tropospheric photochemistry scheme (Folberth et al., 2006; Hauglustaine et al., 2004, 2014). The photolysis reaction of COS in the stratosphere is not considered: the lifetime of COS in the stratosphere is 64 years (Barkley et al., 2008). The model is set up at a horizontal resolution of 3.8° x 1.9° (96 grid cells in longitude and latitude) with 39 hybrid sigma-pressure levels reaching an altitude up to about 75 km, corresponding to a vertical resolution of about 200-300 m in the planetary boundary layer. The model timestep is 30 minutes and the output concentrations are 3-hourly averaged.

2.4.2 Atmospheric simulations: sampling methods and data processing

We ran the LMDz6 version of the atmospheric transport model described above for the years 2000 to 2009. The prescribed COS and CO_2 fluxes used as model inputs are presented in Table 1 and Table 2. The GPP estimated by ORCHIDEE (148.1 Gt C yr^{-1}) is on the high range among the model estimates (Anav et al., 2015), with a corresponding high respiration (145.7 Gt C yr^{-1}) to ensure a realistic net ecosystem exchange (Friedlingstein et al., 2019). However, other high GPP estimates can be found in the literature such as Welp et al. (2011) that suggest a

range of 150 to 175 based on $\delta^{18}O$ data. Likewise, Joiner et al. (2018) have proposed a new GPP product, based

265   on satellite data and calibrated on FLUXNET sites, with an estimate around 140 Gt C yr^{-1} for 2007. The fluxes are given as a lower boundary condition of the atmospheric transport model (LMDz), which then simulates the transport of COS and CO_2 by the atmospheric flow. The atmospheric COS seasonal variations are likely to be dominated by the seasonal exchange with the terrestrial vegetation, while the mean mole fractions result from all sources and sinks of COS, some of which are still largely unknown (e.g. ocean fluxes, Whelan et

270   al., 2018). In this study, we only focus on the seasonal cycle and do not attempt to simulate the annual mean value, we thus started from a null initial state. The atmospheric transport is almost linear with respect to the fluxes: the linearity is a property of the atmospheric transport, though it is violated in LMDz because of the presence of slope limiters in the advection scheme. Overall, since all the other LMDz components are linear, LMDz transport is generally considered linear with fluxes (Hourdin and Talagrand, 2006). Relying on this relationship, we first

275   transported each flux separately, and then added all the simulated concentrations in the end, for each species.

For all COS and CO_2 observations, the model output was sampled at the nearest grid point and vertical level to each station, and was extracted at the exact hour when each flask sample had been taken. For each station, the curve-fitting procedure developed by the NOAA Climate Monitoring and Diagnostic Laboratory (NOAA/CMDL) (Thoning, 1989) was applied to modelled and observed COS and CO_2 time series to extract a smooth detrended

280   seasonal cycle. We first fitted a function including a second-order polynomial term and 4 harmonic terms, and then applied to the residuals a low pass filter with either 80 or 667 days as short-term and long-term cut-off values, respectively. The detrended seasonal cycle is defined as the smooth curve (full function plus short-term residuals) minus the trend curve (polynomial plus long-term residuals).

285   **Table 1: Prescribed COS surface fluxes used as model input. Mean magnitudes of different types of fluxes are given for the period 2000-2009**

*A bug has been discovered in the parameterization of direct COS emissions in the NEMO PISCES ocean model: the hydrolysis rate was three times too low, resulting in an artificial build-up of COS in seawaters. As a correction, we divided by three the total amount of oceanic COS fluxes within a year, assuming that the bug does not affect the spatial pattern of direct emissions
290   of COS.

Type of COS flux	Temporal resolution	Total (Gg S yr^{-1})	Data Source
Anthropogenic	Monthly, interannual	337.3	Zumkehr et al. (2018)
Biomass burning	Monthly, interannual	56.3	Stinecipher et al. (2019)
Soil	Monthly, climatological	-409.0	Launois et al. (2015b)
Ocean	Monthly, climatological	444.7	Kettle (2002) for indirect oceanic emissions (via CS2 and DMS oxydation), and Launois et al. (2015a) for direct oceanic emissions. The direct emissions are rescaled to be equal to 200 Gg S yr^{-1} (*).
Vegetation uptake	Monthly, interannual	See Table 6.	This work, including mechanistic and LRU

			approaches (Seibt et al., 2010; Whelan et al., 2018).

Table 2: Prescribed CO₂ surface fluxes used as model input. Mean magnitudes of different types of fluxes are given for the period 2000-2009

Type of CO₂ flux	Temporal resolution	Total (Gt C yr⁻¹)	Data Source
Fossil fuel	Monthly, interannual	7.7	ECJRC/PBL EDGAR version 4.2
Biomass burning	Monthly, interannual	1.9	GFED 4.1s
Respiration (including the land use emissions and wood harvest)	Monthly, interannual	145.7	ORCHIDEE
Ocean	Monthly, climatological	-1.3	Landschützer et al. (2015)
GPP	Monthly, interannual	-148.1	ORCHIDEE

2.4.3 COS and CO₂ concentrations at the NOAA/Global Monitoring Laboratory surface sites

295   We used the NOAA/GML measurements of both CO₂ and COS at 10 sites located on both hemispheres, listed in Table 3.

Table 3: List of air sampling sites selected for evaluation of COS and CO₂ concentrations

Site	Short name	Coordinates	Elevation (m above sea level)	Comment
South Pole, Antarctica, United States	SPO	90.0°S, 24.8° W	2810	
Cape Grim, Australia	CGO	40.4°S, 144.6°W	164	inlet is 70 m aboveground
Tutuila, American Samoa	SMO	14.2°S, 170.6°W	77	
Cape Kumukahi, United States	KUM	19.5°N, 154.8°W	3	
Mauna Loa, United States	MLO	19.5°N, 155.6°W	3397	
Niwot Ridge, United States	NWR	40.0°N, 105.54°W	3475	
Wisconsin, United States	LEF	45.9°N, 90.3°W	868	inlet is 396 m aboveground on a tall tower
Mace Head, Ireland	MHD	53.3°N, 9.9°W	18	
Barrow, United States	BRW	71.3°N, 155.6°W	8	
Alert, Canada	ALT	82.5°N, 62.3°W	195	

300   The samples are collected as pair flasks one to five times a month since 2000 and are then analysed in the NOAA/GML's Boulder laboratories with gas chromatography and mass spectrometry detection. The measurements are retained only if the difference between the pair flasks is less than 6.3 ppt for COS. These measurements can be downloaded from the ftp sites ftp://ftp.cmdl.noaa.gov/hats/carbonsulfide/ and, for CO₂, at ftp://ftp.cmdl.noaa.gov/ccg/co2.

9

305 **2.4.4 Evaluation metrics**

To evaluate and compare the performances of the mechanistic and LRU approaches at different NOAA surface sites, we used the normalised standard deviation (NSD) and the Pearson correlation coefficient (R). NSD is calculated as the ratio between the standard deviation of the simulated concentrations and the observed concentrations at the NOAA surface sites. NSD and R values closer to 1 indicate a better accuracy of the model.

310 **3 Results**

3.1 Site scale conductances and COS fluxes

3.1.1 Modelled conductances

To investigate the importance of each conductance in vegetation COS uptake we compared the three simulated conductances: leaf boundary layer, stomatal and internal, studying their variability and their environmental drivers

315 at the diel and seasonal scales. The boundary layer conductance to COS is higher than the two other conductances by a factor on the order of 50 (see Table A1 for more detailed statistics). As a high conductance value is equivalent to a low resistance to COS transfer, we focused only on the stomatal (g_{S_COS}) and internal (g_{I_COS}) conductances, which are the two most limiting factors to plant COS uptake.

a) Diel cycles of g_{S_COS} and g_{l_COS} for each month at the Harvard site in 2012

b) Diel cycles of g_{S_COS} and g_{l_COS} for each month at the Hyytiala site in 2017
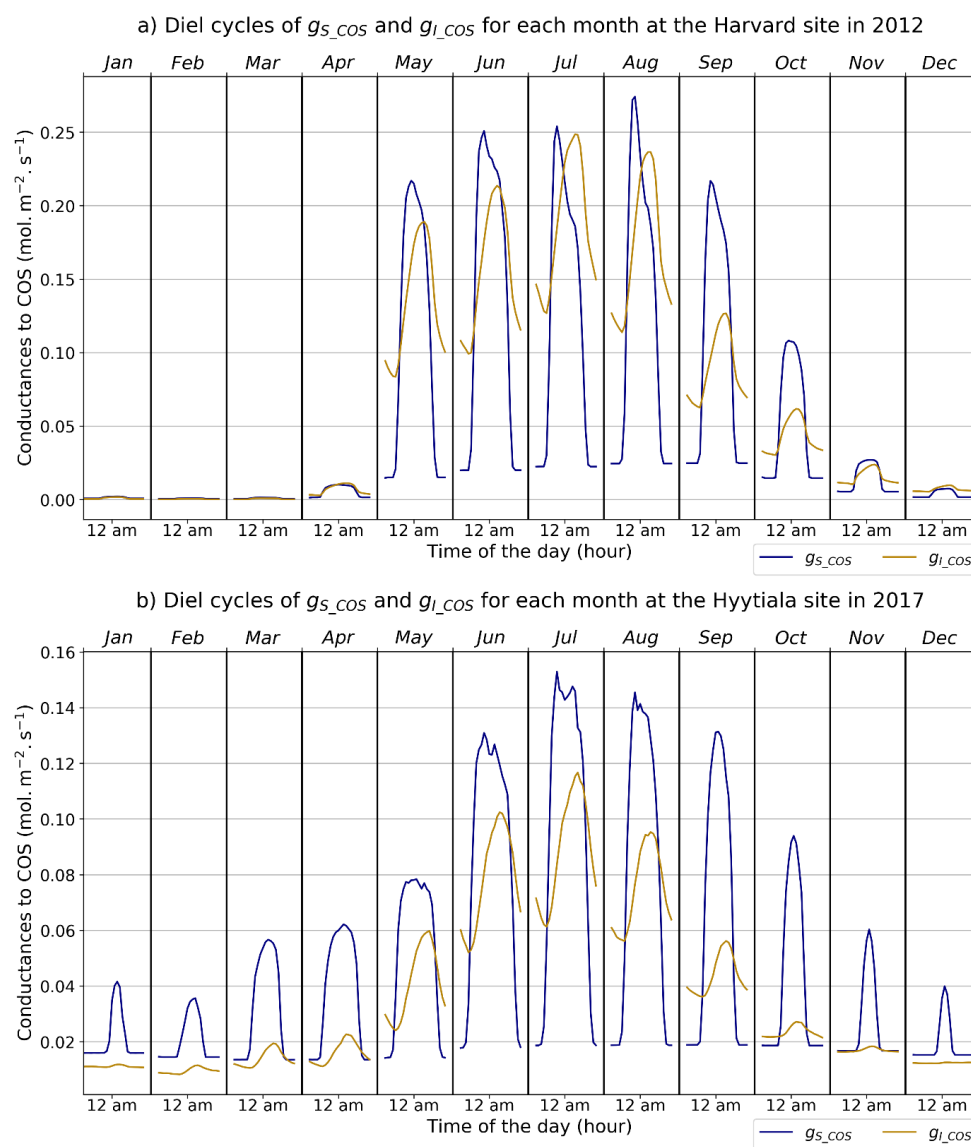

Figure 1: Mean diel cycles of simulated conductances for each month for Harvard Forest in 2012 (a) and Hyytiälä in 2017 (b)

Figure 1 presents the mean diel (i.e. 24-hourly) cycles of the internal and stomatal conductances for each month, computed over 2012 at Harvard Forest and 2017 at Hyytiälä. The two conductances follow the same seasonal variations. Both increase during the growing season when vegetation becomes active and reach a maximum in July. Then, the conductances start to decline to a minimum value in winter. Harvard Forest is predominantly a deciduous forest and winter values of the two conductances are zero at this site as there are no leaves in that season. Hyytiälä on the other hand is an evergreen pine forest, such that daytime stomatal conductance in winter does not become zero. Diel variations at both sites are represented by a rise in both conductances in the morning with a

maximum around midday. The conductances drop in the afternoon to reach minimum values at night. However,
330   between May and September, there is an inversion of the limiting conductance depending on the time of the day.
The internal conductance is lower than the stomatal conductance in the morning and until early afternoon, while
the stomatal conductance is the lowest at night. Moreover, in summer, the amplitude of diel variations of the
internal conductance is lower than the amplitude of diel variations for the stomatal conductance. Also, the
nighttime minimum value of the internal conductance displays larger seasonal variations than that of the stomatal
335   conductance.

To understand the shift of dominance between the two conductances during nighttime and daytime, we looked at
the strength of covariation between the simulated conductances and environmental variables directly or indirectly
involved in their modelling: air surface temperature (T_{air}), photosynthetically active radiation (PAR), vapor
340   pressure deficit (VPD) and soil moisture (SM). The results are presented for the Hyytiälä site as an example.
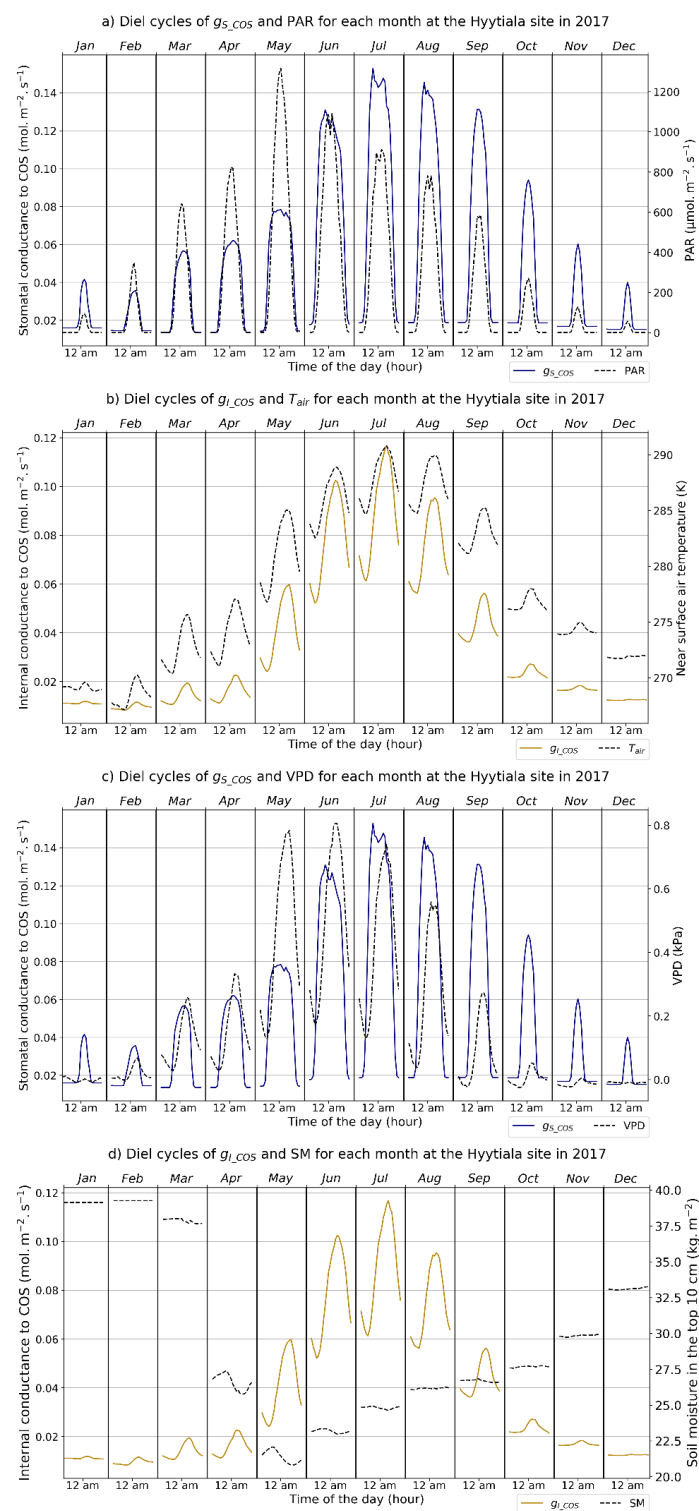
Figure 2: Mean diel cycle of simulated conductances and their environmental drivers for each month at Hyytiälä (2017). a) PAR and stomatal conductance, b) air temperature and internal conductance, c) VPD and stomatal conductance, d) soil moisture and internal conductance.

The simulated stomatal conductance, g_{S_COS}, is linearly related to the CO_2 assimilation, which depends mainly on PAR, and g_{S_COS} also depends on VPD (Yin and Struik, 2009). g_{S_COS} and PAR show the same variations for diel and seasonal cycles, and the daily maximum values occur at the same time (Figure 2a). Computing coefficients of determination, we found that 64% of the g_{S_COS} variance is explained by PAR, while 32% of the simulated internal conductance variance is explained by PAR. The mean diel cycle of g_{S_COS} and VPD (Figure 2c) also show similar diel variations but we notice that diel cycles of the g_{S_COS} are ahead of VPD diel cycles, except in winter where diel cycles differ between g_{S_COS} and VPD. VPD explains 47% of the stomatal conductance variance and 67% of the internal conductance.

The simulated internal conductance, g_{I_COS}, is proportional to V_{max}, which represents the Rubisco activity for CO_2. V_{max} is assumed to be a measure for the CA activity for COS, and depends on T_{air} and SM in the model. The mean diel cycles of the simulated g_{I_COS} and of T_{air} follow the same variations and show the same amplitude (Figure 2b). 90% of the g_{I_COS} variance is explained by T_{air}, while 50% of the g_{S_COS} variance is explained by T_{air}. g_{I_COS} and SM show similar diel variations in spring and summer (Figure 2d). SM and the conductances are anti-correlated as water loss by transpiration will rise with increasing conductances (as well as soil evaporation with increasing temperatures). SM explains 44% of the g_{I_COS} variance while it explains only 22% of the g_{S_COS} variance.

Partial correlations presented in Table 4 also confirm the dominance of PAR (0.61) and T_{air} (0.54) on g_{S_COS} response, while T_{air} (0.84) and VPD (0.55) are the main environmental factors for g_{I_COS}. This explains why g_{I_COS} is more limiting in winter because T_{air}, is low with thus lower enzyme activities, considering here T_{air} as a proxy of the leaf temperature, and as soon as T_{air} rises in spring the g_{I_COS} becomes less limiting.

Table 4: Partial correlations between conductances and environmental drivers

	PAR	T_{air}	VPD	SM
g_{S_cos}	0.61	0.54	-0.30	0.04
g_{I_cos}	-0.11	0.84	0.55	0.25

Biogeosciences
Discussions
Open Access
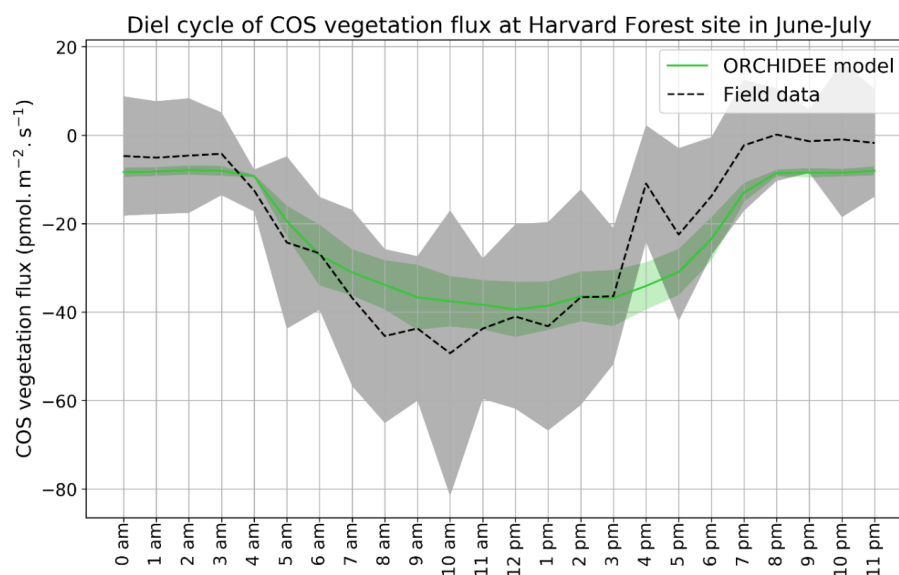EGU

3.1.2 COS fluxes

3.1.2.1 Daily cycle

Figure 3: Mean diel cycle of observed vegetation COS flux (Wehr et al., 2017) and modelled COS vegetation flux in June and July 2012 and 2013 (Harvard Forest) using an atmospheric convention where an uptake of COS by the ecosystem is negative. The shaded areas above and below each curve represent one standard-deviation of the considered hourly values over the June-July period.

COS assimilation is minimum at night (between 8 PM and 4 AM) for observed and simulated fluxes (Figure 3). During night, uptake of modelled COS flux is around -8 pmol m^{-2} s^{-1} while field observations vary between -5 pmol m^{-2} s^{-1} and 0 pmol m^{-2} s^{-1}. In the morning, both simulated and observed uptakes increase. However, while the simulation shows a maximum assimilation of -38 pmol m^{-2} s^{-1} at noon, the maximum assimilation for observations is reached at 10 AM with a flux of -49 pmol m^{-2} s^{-1}. Observed fluxes have thus a greater daily amplitude than simulated fluxes, and are a little ahead of the simulation, but this shift does not seem significant given the large variability of observations, as represented by the one standard-deviation in Figure 3. We notice that the simulated diel cycle of COS flux is similar to the ones of the stomatal and internal conductances, with a stronger limitation by the internal conductance in the morning. RMSD for this mean diel cycle is 8.0 pmol m^{-2} s^{-1}, and relative RMSD is 35%. A similar study at the Hyytiälä site over May-November in year 2015 yields a similar underestimation of the amplitude of the mean diel cycle, with an RMSD of 4.0 pmol m^{-2}·s^{-1} and a relative RMSD of 36%.
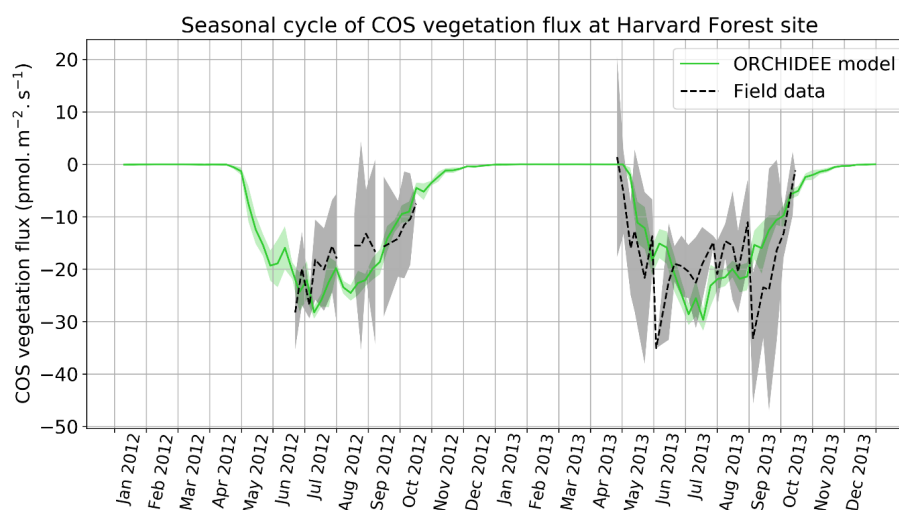
3.1.2.2 Seasonal cycle

Figure 4: Mean seasonal cycle of simulated and observed weekly average vegetation COS flux in 2012 and 2013
390 **(Harvard Forest). The shaded areas above and below each curve represent one standard-deviation of the daily means within the considered week.**

The simulated weekly seasonal vegetation COS uptake follows the same trend as the observed one (Figure 4).

COS uptake increases in spring when the vegetation growing season starts and decreases in autumn at the end of

the forest activity period. Simulated and observed fluxes also take similar values over the two years. We notice

395 that the amplitude of observed COS flux variations is larger than the one of modelled fluxes. The use of the eddy

covariance method for field measurements can create noise, which could explain the larger fluctuations for field

data. RMSD for the seasonal cycle is 7.5 pmol m^{-2} s^{-1}, and the relative RMSD is 44%. At the Hyytiälä site over

May-November in year 2015, the RMSD for the seasonal cycle is 2.4 pmol m^{-2} s^{-1}, and the relative RMSD is 25%.
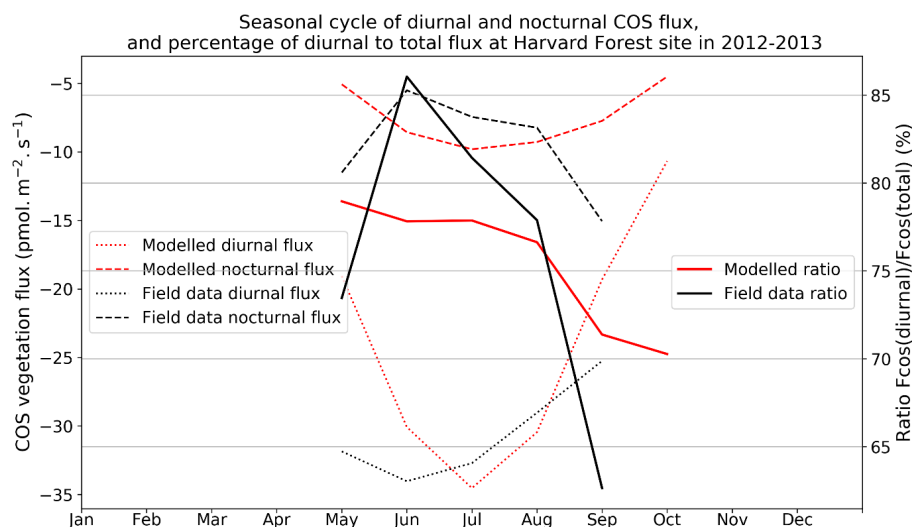
3.1.2.3 Nighttime fluxes

Figure 5: Seasonal cycle of diurnal (dotted curve) and nocturnal (dashed curve) for observed (black) and modelled (red) vegetation COS fluxes, with the percentage of the diurnal to the total flux (solid curve) at Harvard Forest in 2012-2013

Figure 5 compares mean diurnal and nocturnal observed and modelled vegetation COS fluxes and the percentage of the diurnal to the total flux, computed for each month over 2012 and 2013 at the Harvard Forest site. We selected an arbitrary PAR threshold of 50 μmol m^{-2} s^{-1} to split between diurnal and nocturnal fluxes. We see that the modelled nocturnal flux varies across the growing season, with a maximum uptake of -8 pmol m^{-2} s^{-1} reached in July and August and a lower assimilation in the enclosing colder months. This seasonal variation can be explained by the seasonal change in leaf area index (LAI) and the conductances dependency on T_{air}, which increases in summer. The observed nighttime fluxes are of the same magnitude but present an opposite seasonal cycle with lower uptake at the summer peak, albeit variations are within the one-standard deviation represented in Figure 3. The modelled nighttime fluxes account for 20 to 30% of the total COS uptake. The observed ones exhibit a larger range, between 5 and 40%. Kooijmans et al. (2017) found a ratio of 21% at the Hyytiälä site. These ratios are in line with other studies: Maysek et al. (2014) reported a ratio of 29 ± 5% over a wheat field in Oklahoma, and Sun et al. (2018b) one of 23% for the San Joaquin Freshwater Marsh site in California. The results may vary given the definitions adopted for nighttime and daytime periods.

3.1.3 LRU as a function of PAR

LRU decreases as a function of PAR, as initially observed by Stimler et al. (2010). Kooijmans et al. (2019) made measurements in two branch chambers installed at the top of the canopy in two Scots pine trees in Hyytiälä. They plotted the response of LRU to light, as quantified by the photosynthetically active radiation (PAR). To compare the ORCHIDEE model behaviour to these field data, we determined an LRU using our modelled COS and GPP fluxes, considering a constant atmospheric concentration of 500 ppt for COS and global yearly values for CO$_2$.
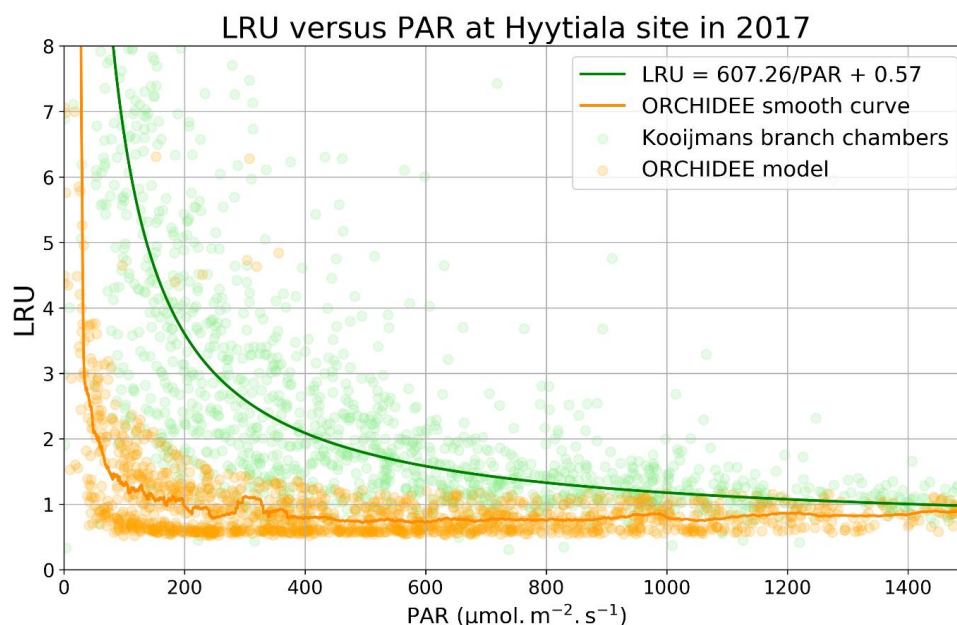
17

Figure 6: LRU against PAR (Hyytiälä) for ORCHIDEE outputs and measurements (hourly data measured between 18 May and 13 July, Kooijmans et al., 2019). The light green circles represent average LRU values for chambers 1 and 2, light orange circles represent modelled LRU values. A moving average with a window of 50 points leads to the orange smooth curve for the model. The green line represents the function LRU=607.26/PAR + 0.57 from Figure S6 of the Kooijmans et al. (2019) supplement. To focus on LRU behaviour when PAR decreases, we plotted LRU response to PAR for PAR < 1500 µmol m^{-2} s^{-1}.

LRU increases with low PAR values for both branch chambers and for the model, and converge towards a constant value for high PAR values (Figure 6). This demonstrates that assuming a constant value for LRU, and not considering an increase in LRU under low light conditions, will result in erroneous estimation of COS fluxes. The increasing LRU can be explained by the light-dependence of the photosynthesis reaction contrary to the CA activity that is light-independent. Consequently, CO_2 fluxes tend to zero when PAR decreases while COS is still taken up in the dark, leading in theory to infinite values of LRU. It is to be noted that the drop of LRU when PAR increases is much sharper in the model that in the observations.

3.2 Global scale plant COS fluxes and Study of LRU values

3.2.1 Comparison of plant COS uptake sink estimates
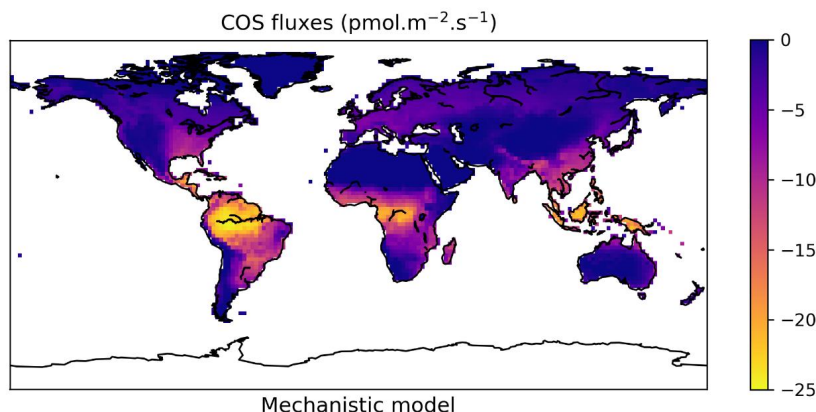

440

Figure 7: Map of average vegetation COS fluxes over the 2000-2009 period, from the mechanistic model as implemented in ORCHIDEE

The mechanistic approach simulated in the ORCHIDEE model gives a plant COS uptake of -756 Gg S yr^{-1} over the 2000-2009 period. COS fluxes are the strongest in South America, Central Africa and Southeast Asia (Figure

445   7), as expected as these regions are also the most productive ones for GPP.

Table 5: Overview of COS plant uptake per year (Gg S yr^{-1})

	Kettle et al. (2002)	Montzka et al. (2007)	Suntharalingam et al. (2008)	Berry et al. (2013)	Launois et al. (2015b)			This study
					ORC.	LPJ	CLM4	
Uptake by plants	-238 (±30)	-730 to -1500	-490 (-460 to -530)	-738	-1335	-1069	-930	-756

The more recent studies (Montzka et al., 2007; Suntharalingam et al., 2008; Berry et al., 2013; Launois et al.,

450   2015b) show a higher global plant sink than the one initially found by Kettle et al. (2002) (Table 5). Kettle et al. (2002) used an LRU-like approach, based on NPP and on the NDVI temporal evolution, and already acknowledged their estimate was assumed to be a lower bound one. Estimates from plant chambers and atmospheric measurements (Sandoval et al., 2005; Montzka et al., 2007; Campbell et al., 2008) confirmed that the COS plant sink should be twofold to fivefold larger than estimated in Kettle et al. (2002). Sutharalingham et al. (2008) also

455   found a low estimate of -490 Gg S yr^{-1}, using 3D modelling of COS atmospheric concentrations, constrained by surface site observations. We note that our estimate is similar to the -738 Gg S yr^{-1} found by Berry et al. (2013), which was implemented in the Simple Biosphere (SiB) 3 LSM. The reason for this similarity can be that the leaf photosynthesis and stomatal conductance in both LSMs are derived from the same classical models from Farquhar et al. (1980), Collatz et al. (1992) and Ball et al. (1987).

460   Launois et al. (2015b) adopted an LRU approach, using constant LRU values for large MODIS vegetation classes, adapted from Seibt et al. (2010). Based on these values and a set of global GPP estimates from three LSMs

19

(ORCHIDEE, LPJ, CLM4), the authors derived the corresponding global vegetation COS uptakes reported in Table 5. The selection of the LSM itself thus introduces an uncertainty on the global vegetation COS uptake of around 40% in this case.

465   Applying the LRU values derived from Seibt et al. (2010) (Table 6) to the global GPP simulated in this study leads to the highest plant COS uptake with -1343.3 Gg S yr^{-1}. Seibt et al. (2010) report LRU values for different internal conductance limitations. The LRU values that we used here represent a small limitation of internal conductance to the total COS uptake (the ratio of stomatal to internal conductances is 0.1). A smaller global COS uptake can be expected when the LRU values with a more limiting effect of the internal conductance are used. Applying the

470   LRU values derived from Whelan et al. (2018) (Table 6) leads to an intermediate estimate of -808.3 Gg S yr^{-1}, which is closer to the global uptake obtained with the mechanistic model. This analysis shows that the choice for certain LRU values introduces an uncertainty on the global vegetation COS uptake (around 70% in this case), and highlights the importance of deriving accurate PFT-dependent LRU values.

3.2.2 Dynamics of simulated LRU values

475   The PFT distributions of the LRU values, computed using a monthly climatology of mechanistic COS and GPP fluxes over the 2000-2009 period, do not support the idea of a constant PFT-dependent LRU value (Figure 8).
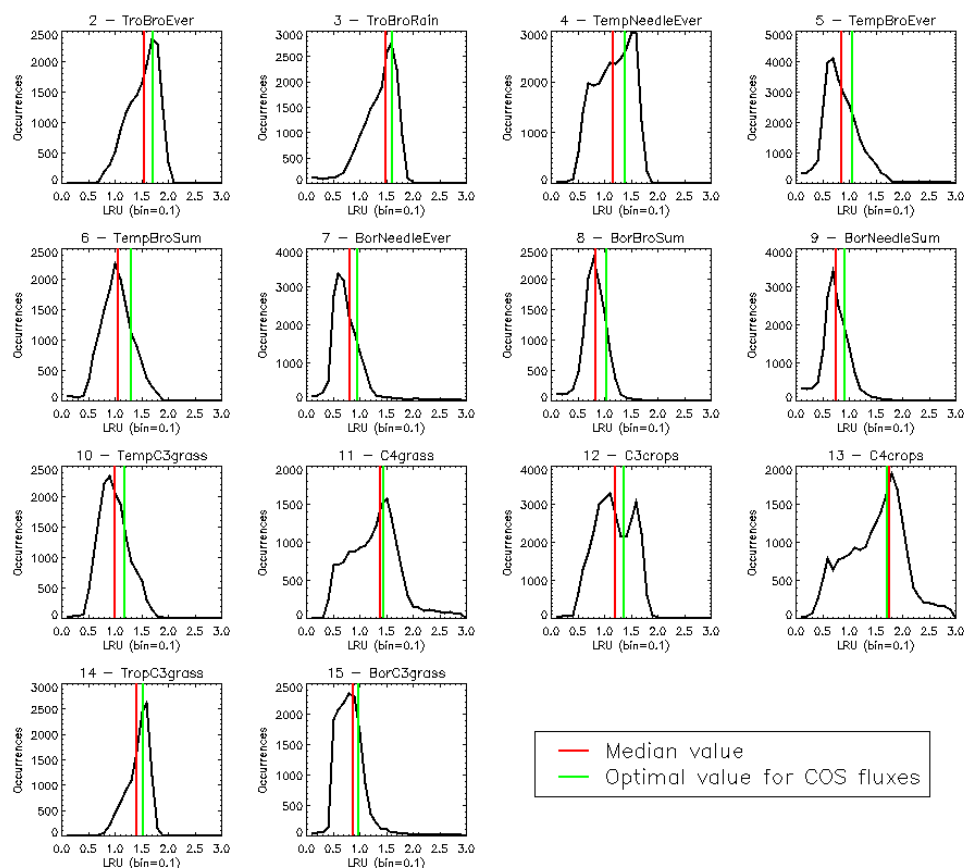
Figure 8: Distributions of the LRU values computed from the mechanistic approach, using a monthly climatology of simulated COS and GPP fluxes over the 2000-2009 period. Each subplot represents one of the 14 vegetated PFTs used 480 **in ORCHIDEE, considering all grid cells where the PFT is present. The x-axis represents the LRU value between 0 and 3, with 0.1 bins. The y-axis represents the occurrences. For each PFT, the red vertical bar represents the median LRU value, the green vertical bar represents the LRU optimal value that minimizes the error between plant COS uptakes estimated by the mechanistic approach and the LRU approach for all pixels of the considered PFT (see names and abbreviations in Table 6).**

485 The distributions are usually not gaussian; nor are they all unimodal, as is the case for PFT 12 C3 Agriculture. The

distributions for C4 PFTs (PFT 11 C4 Grass and PFT 13 C4 Agriculture) exhibit a large spread. The median values

are represented by vertical red bars in Figure 8 and listed in Table 6. The optimal values (LRU_Opt) obtained by

linearly regressing COS fluxes against GPP multiplied by the ratio of the mean COS to CO_2 concentrations (see

Figure B1) are represented by vertical green bars and also listed in Table 6. They are usually higher than the

490 median values, with a mean difference of 12.1%. Using either monthly means or yearly means of fluxes gives very

similar optimal LRU values, the mean difference being only -0.2%.

Table 6: Table of LRU per PFT. First column: median and optimal LRU values calculated from the simulated mechanistic COS and GPP fluxes. Middle columns: calculated from Seibt et al. (2010) for the ORCHIDEE PFT 495 **classification. Last column: from Whelan et al. (2018)**

PFT		ORCHIDEE		Seibt	Whelan
Long name	Abbreviation	Median	Optimal		
1 - Bare soil	Bare	0.00	0.00	0.00	0.00
2 - Tropical Broad-leaved Evergreen Forest	TroBroEver	1.56	1.72	3.09	1.68
3 - Tropical Broad-leaved Raingreen Forest	TroBroRain	1.48	1.62	3.38	1.68
4 - Temperate Needleleaf Evergreen Forest	TempNeedleEver	1.17	1.39	1.89	1.68
5 - Temperate Broad-leaved Evergreen Forest	TempBroEver	0.86	1.06	3.60	1.68
6 - Temperate Broad-leaved Summergreen Forest	TempBroSum	1.06	1.31	3.60	1.68
7 - Boreal Needleleaf Evergreen Forest	BorNeedleEver	0.82	0.95	1.89	1.68
8 - Boreal Broad-leaved Summergreen Forest	BorBroSum	0.84	1.03	1.94	1.68
9 - Boreal Needleleaf Summergreen Forest	BorNeedleSum	0.76	0.92	1.89	1.68
10 - Temperate C3 Grass	TempC3grass	1.01	1.18	2.53	1.68
11 - C4 Grass	C4grass	1.38	1.45	2.00	1.21
12 - C3 Agriculture	C3crops	1.21	1.37	2.26	1.68
13 - C4 Agriculture	C4crops	1.75	1.72	2.00	1.21
14- Tropical C3 grass	TropC3grass	1.40	1.52	2.39	1.68
15- Boreal C3 grass	BorC3grass	0.87	0.97	2.02	1.68

LRU_Opt values are much smaller than LRU_Seibt values for all PFTs, roughly by a factor 2. They are closer to

the LRU_Whelan values, being smaller for all C3 PFTs except the Tropical Broad-leaved Evergreen Forests, and

higher for C4 PFTs (Table 6). In the LRU_Opt set, the most productive PFTs (tropical forests and C4 crops) have

500 the highest values around 1.7, while the less productive PFTs (boreal forests and grasses) have the lowest values

around 0.9. To the contrary, in the LRU_Seibt set, temperate broad-leaved forests have the highest values (3.6) while needleleaf forests have the smallest value around 1.9.

Another way to understand the distribution of LRU values is to look directly at the scatter plots of monthly COS

505   fluxes against GPP fluxes, multiplied by the ratio of COS to CO_2 concentrations (Figure B1). For most PFTs, it is in fact obvious that the relationship shows non-linear features, disagreeing with the classical linear LRU model. Based on these findings, we fitted a simple exponential model as:

$$F_{COS} = a \left(e^{bGPP\frac{[COS]_a}{[CO_2]_a}} - 1 \right)$$

with two parameters a and b. However, given the large spread of the data around the model, the Akaike criteria is

510   always favourable to the LRU linear model, so we won't investigate further with this exponential model, more specific research is needed here in order to bridge this data gap. Still, it is important to note that the larger COS fluxes will in general be underestimated using a linear LRU approach. It also appears that in certain PFTs (4, 5, 7) small COS fluxes will be underestimated.

515   We computed mean annual vegetation COS fluxes using our modelled GPP and this new *LRU_Opt* set of values and compared them to the mechanistic COS fluxes (Figure 9a).
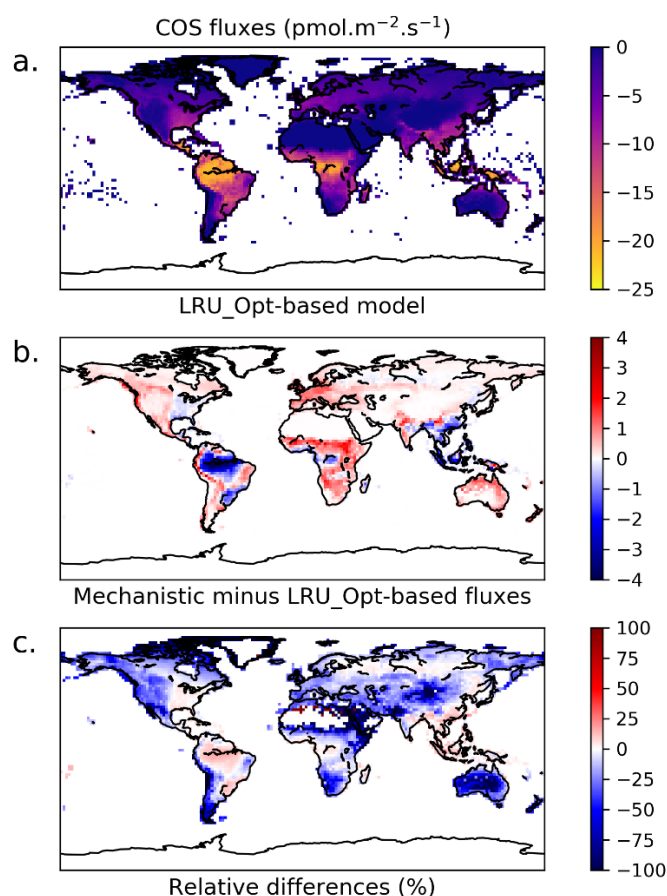
Figure 9: a. Mean annual vegetation COS fluxes for the 2000-2009 period fluxes computed using a linear LRU approach with optimal values for each PFT. b. Differences between mechanistic and LRU-based fluxes. c. Relative differences (%)

520

The maps of differences between the mechanistic and *LRU_Opt*-based COS fluxes (Figure 9b), and relative differences (Figure 9c), provide evidence for the spatial errors introduced by considering a constant LRU value. The differences are always lower than 4 pmol m^{-2} s^{-1} in absolute values, and are mainly positive, with the main exception over the Amazon region where the mechanistic approach shows a larger uptake than the linear LRU

525 approach. The difference between the global estimates of the two approaches is less than 2%; we could still improve the linear regression determining the LRU optimal value by weighting grid-cell fluxes with the corresponding surface of the PFT.

We also compared the mean seasonal cycles of the COS vegetation flux over the 2000-2009 period, for the mechanistic approach and the *LRU_Opt*-based approach, for each PFT (Figure 10). The seasonal cycles are very

530 similar; for PFT 13 C4 Agriculture, the *LRU_Opt*-based cycle is slightly in advance as compared to the mechanistic cycle.
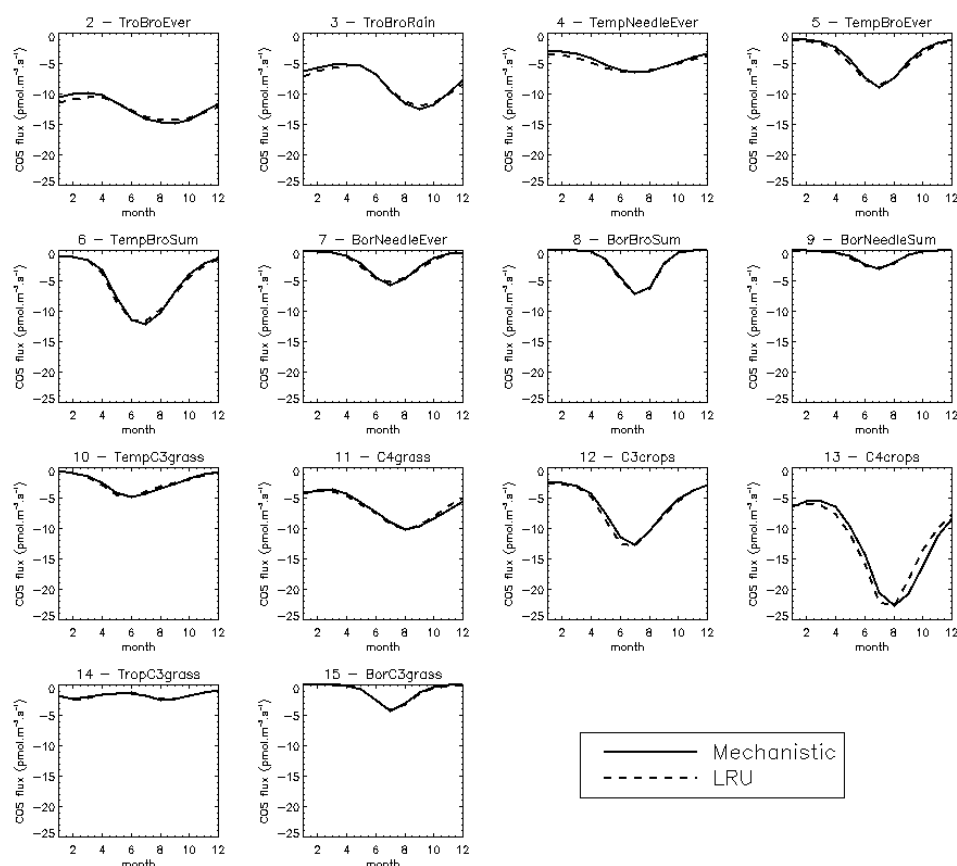
Figure 10: Mean seasonal cycle (monthly means) of COS for each PFT over the Northern hemisphere for the 2000-2009 period. The solid line represents the mechanistic model, while the dashed line represents the optimal LRU approach.

535 **3.3 Simulating atmospheric COS concentration at surface stations**

We transported the global COS and CO_2 fluxes (i.e. the ones obtained from the ORCHIDEE model plus the additional components of each cycle, listed in Table 1 and Table 2) with the LMDz6 atmospheric transport model as described in Sect. 2.4.2. We analysed COS concentrations derived from simulated COS fluxes obtained with the mechanistic and LRU approaches in regards with observed COS concentrations from the NOAA at a few
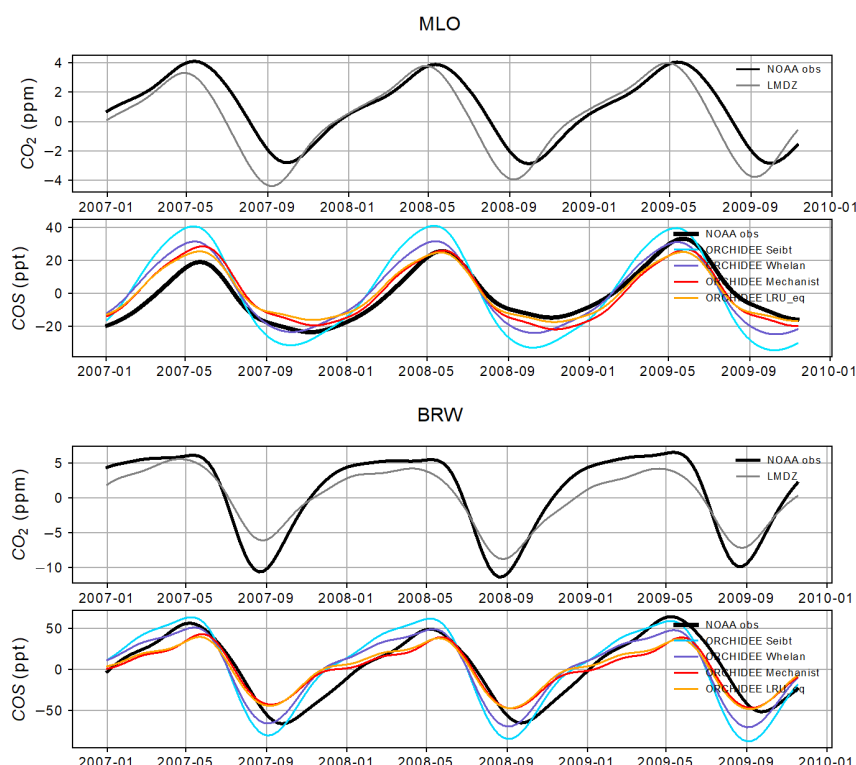
540 selected sites.

Figure 11: Detrended temporal evolutions of simulated and observed CO₂ and COS concentrations at two selected sites, for the mechanistic (ORCHIDEE Mechanist) and LRU approaches (ORCHIDEE Seibt, ORCHIDEE Whelan, ORCHIDEE LRU_eq), simulated with LMDz6 transport between 2007 and 2009. The ORCHIDEE LRU_eq line (orange) corresponds to the concentrations simulated using the optimal LRU values derived from the mechanistic model. Top: Mauna Loa station (MLO, Hawaii), bottom: Barrow station (BRW, Canada). The curves have been detrended beforehand and filtered to remove the synoptic variability (see Sect. 2.2.4)

Figure 11 shows the detrended temporal evolution of CO₂ and COS concentrations for the mechanistic and LRU approaches at Barrow (BRW, Canada) and Mauna Loa (MLO, Hawaii). The MLO site samples air masses coming from all over the northern hemisphere (Conway et al., 1994). CO₂ seasonal amplitude at BRW reflects the contributions of surface fluxes from high latitude ecosystems (Peylin et al., 1999), but also from regions further south due to atmospheric transport (Parazoo et al., 2011; Graven et al., 2013). These two stations have been used to detect large-scale changes in ecosystem functioning (Graven et al., 2013; Commane et al., 2017). In spite of their importance, LMDz driven by the ORCHIDEE vegetation fluxes has difficulties in representing their seasonal cycles. For instance, at MLO, the simulated seasonal amplitude of CO₂ is overestimated and precedes the observations by one month.

For COS, the simulated concentrations match relatively well the observed seasonal variations and seem to be more in phase with the observations than for CO₂. Such a feature could indicate that the phase issues with CO₂ is not primarily driven by GPP issues but by the other CO₂ flux components. The mechanistic model and its LRU optimal equivalent better reproduce the observed one-month lag between the COS and the CO₂ simulation at MLO (i.e. the minimum COS lags the one of CO₂) than the other LRU approaches (Whelan and Seibt). The simulations differ more in the amplitude than in the phase of their seasonal cycles. The mechanistic approach simulates an amplitude

25

lower than the LRU ones. At MLO for example, the lower amplitude of the mechanistic model is in better
agreement with the observations. At BRW, its seasonal amplitude is also lower but is now underestimated. The
565   COS concentration at this station from the mechanistic approach varies between +30 ppt and -50 ppt while it varies
between +50 ppt (respectively +37) and -71 ppt (respectively -50) for the simulation based on Seibt et al. (2010)
(respectively Whelan et al., 2018). This is a direct consequence of lower COS fluxes with the mechanistic model
compared to the fluxes based on Seibt and Whelan LRU approaches. At both the MLO and BRW sites, the
difference between the mechanistic model and its LRU optimal equivalent after being transported is lower than 8
570   ppt, within the range of the observations uncertainty.

Table 7: Normalized standard deviations (NSDs) of the simulated concentrations by the observed concentrations. Within brackets are the Pearson correlation coefficients (R) between simulated and observed COS concentrations for the mechanistic and LRU approaches, calculated between 2004 and 2009 at 10 NOAA stations. For each station, NSD
575   **and R closest to one are in bold and farthest ones are in italic. The time-series have been detrended beforehand and filtered to remove the synoptic variability (see Sect. 2.2.4).**

	SPO	CGO	SMO	KUM	MLO	NWR	LEF	MHD	BRW	ALT
ORCHIDEE	*1.15*	*0.67*	**0.58**	1.32	*1.65*	*2.12*	*2.17*	*1.52*	1.25	1.16
Seibt	*(0.96)*	*(0.5)*	(-0.47)	*(0.92)*	*(0.89)*	*(0.50)*	*(0.92)*	**(0.96)**	*(0.90)*	**(0.95)**
ORCHIDEE	**1.00**	0.83	0.40	**1.03**	1.23	1.50	1.67	1.26	**1.00**	**0.92**
Whelan	(0.97)	(0.91)	(0.1)	(0.93)	(0.90)	(0.52)	(0.93)	(0.94)	*(0.90)*	*(0.94)*
ORCHIDEE	1.10	**1.01**	*0.35*	0.90	**1.05**	1.26	**1.34**	1.09	0.69	*0.64*
mechanist	(0.97)	**(0.97)**	**(0.4)**	**(0.95)**	**(0.92)**	**(0.63)**	**(0.94)**	*(0.85)*	**(0.91)**	**(0.95)**
ORCHIDEE	1.02	0.98	0.34	*0.85*	0.94	**1.21**	**1.34**	1.04	*0.68*	*0.64*
LRU_eq	**(0.98)**	**(0.97)**	*(-0.5)*	(0.94)	**(0.92)**	*(0.50)*	**(0.94)**	(0.88)	**(0.91)**	**(0.95)**

Table 7 presents the NSDs and Pearson correlation coefficients between simulated and observed COS
concentrations for the mechanistic and LRU approaches. We see that the simulation with Seibt et al. (2010)
580   intermediate LRU values overestimates the seasonal standard deviation and has the lowest accuracy for most
stations. It is difficult to tell whether the mechanistic model is better than the LRU approach based on Whelan
values. While the mechanistic approach captures known features of the temporal dynamics of the COS to CO_2 flux
ratio, it underestimates the simulated concentrations at Alert (ALT, Canada) and Barrow (BRW, United States). It
should be noted that, due to other sources of errors (in particular transport and oceanic emissions), the comparison
585   presented here should be taken as a sensitivity study of COS seasonal cycle to the vegetation scheme rather than
a complete validation of one approach.

4 Discussion

4.1 How can we use COS fluxes and the mechanistic COS model to improve the simulated GPP?

The mechanistic model links vegetation COS uptake and GPP fluxes through the stomatal conductance model,
590   which includes the minimal conductance as an offset, and the common use of the carboxylation rate of Rubisco,
V_{max}, in the internal conductance formulation for COS, and in the Rubisco-limited rate of assimilation for CO_2.
The downside is the introduction of the somewhat uncertain α parameter that relates the COS internal conductance
to V_{max}. Using COS flux measurements to optimize the parameters of the stomatal and internal conductances

would thus in principle benefit the simulated GPP. This optimization may be done based on appropriate data
595   assimilation techniques; for example, Kuppel et al. (2012) optimized key parameters of the ORCHIDEE model
related to several processes including photosynthesis (see their Table 2), by assimilating eddy-covariance flux data
over multiple sites. The approach relies on a Bayesian framework where a cost function including uncertainties on
observations, model and parameters is minimized (Tarantola, 1987). The results obtained in this study pave the
way for a similar approach using COS fluxes to optimise key parameters controlling GPP; they can be used to
600   define an optimal set up for the a priori errors and the error correlations in a Bayesian framework.

4.1.1 First step: Improving the mechanistic modelling of vegetation COS fluxes

The chosen mechanistic model was able to reproduce observed vegetation COS fluxes at the Harvard Forest and
Hyytiälä sites with RMSDs on the order of 40% without any calibration. However, at the Harvard Forest site, the
diel cycles differ from the ones obtained in Wehr et al. (2017), derived from flux measurements (their Figure 4),
605   and somewhat validated by the close agreement between two different methods (one from COS flux and one from
water flux). The stomatal conductance in the ORCHIDEE model peaks more sharply in the morning, and the
modelled internal conductance is lower and more variable than in Wehr et al. (2017). Diel variations in atmospheric
$[COS]_a$, not accounted for in our model, cannot explain these differences, as they would only affect F_{COS} but not
the conductances. These discrepancies indeed advocate for the assimilation of COS fluxes to optimize the
610   parameters related to the internal and stomatal conductances. In our modelling framework, the internal
conductance is assumed to be the product of V_{max} by the α parameter. This parameter has been calibrated by Berry
et al. (2013) using gas exchange measurements of COS and CO_2 uptake (Stimler et al., 2010; Stimler et al., 2012).
They estimated two values of α, one for C3 and one for C4 plants, by performing a Type II regression between
modelled COS fluxes and observations. As this α parameter seems much more uncertain as compared to the
615   relatively well known V_{max}, and as it appears only as multiplied by V_{max} in the COS internal conductance
formulation, we should first try to optimize α keeping V_{max} fixed.

4.1.2 Exploiting the alternative dominant role between stomatal and internal conductances

Without being perfect, the mechanistic model could reproduce some expected behaviours. Thus, the mean diel
cycles of simulated conductances for each month at Hyytiälä in 2017 (Figure 1b) show that the internal
620   conductance is the limiting factor from January to April. This result is consistent with Kooijmans et al. (2019) who
found that in the early season the COS flux was limited by the internal conductance. This is explained by low
temperatures that inhibit CA activity and reduce mesophyll diffusion, which are the components of the internal
conductance. Our finding of an inversion of the limiting conductance to COS flux between daytime and nighttime
also agrees with Kooijmans et al. (2019) results, describing a larger effect of the stomatal conductance at night
625   and a limitation of the COS flux by the internal conductance during daytime. Determining the limiting
conductances to COS uptake depending on the time of day provides useful information, as it can be used to better
target which model parameters to optimize, using data assimilation approaches. Thus, observations made in the
morning and early afternoon could be used to better constrain the α parameter when the internal conductance is
limiting COS fluxes, at least as modelled on the C3 species of the two sites, and we could investigate whether the
630   α parameter should be further quantified per PFT rather than simply per photosynthetic pathway. It is to be noted
that for C4 species, the internal conductance is larger than for C3 species by a factor ten, so that stomatal

conductance is limiting, and it could be difficult and useless to try optimizing internal conductance using the α parameter. In addition to optimizing the parameters of the internal conductance, an improvement could be to replace it by the two factors it represents, i.e. the mesophyll conductance and CA activity.

4.1.3 Exploiting nighttime conductances

Recent studies have shown that nighttime field measurements of stomatal conductances often exhibit larger values than the ones used in models (Caird et al., 2007; Phillips et al., 2010). In the ORCHIDEE model, minimum conductances to CO_2 take two different values: 6.25 mmol m^{-2} s^{-1} for C3 species and 18.75 mmol m^{-2} s^{-1} for C4 species. However, Lombardozzi et al. (2017), using data from literature, found that observed nighttime conductances to CO_2 range from 0 mmol m^{-2} s^{-1} to 450 mmol m^{-2} s^{-1} with an overall mean value of 78 mmol m^{-2} s^{-1}. Moreover, they defined a mean value for each PFT (see Table A2) while the ORCHIDEE model uses one value for all C3 species and another one for all C4 species. Using higher nighttime stomatal conductances in models has the impact of increasing plant transpiration and reducing available soil moisture, which alters water and carbon budgets, especially in semi-arid regions (Lombardozzi et al., 2017). Lower VPD values at night, that could limit the impact of higher nitghttime stomatal conductances, follow however an increasing trend (Sadok and Jagadish, 2020). A better representation of these minimal conductances in the model could then improve the constraint of gas exchange between the atmosphere and the terrestrial biosphere. During nighttime, the stomatal conductance limits COS uptake. In the model, the nocturnal stomatal conductance to COS is calculated from the above-mentioned minimum stomatal conductance values. Therefore, nighttime observations of COS fluxes could be used to optimize the minimum stomatal conductance values for each PFT. These minimum values could then be compared to the ones estimated in Lombardozzi et al. (2017).

We thus see that COS fluxes could be used, through standard data assimilation techniques, to optimize the model parameters related to conductances, thus contributing to the improvement of the GPP. However, many more COS flux measurements are needed over a large variety of biomes, first to assert the validity of the mechanistic COS model at global scale, and second to be assimilated in order to improve simulated conductances and GPP estimates.

4.2 The mechanistic versus LRU approach

The mechanistic model is able to reproduce the high temporal frequency LRU variations observed at sites. It is thus legitimate to consider this approach as more accurate than the classical linear LRU approach that uses a time-constant LRU value per PFT to estimate COS fluxes from GPP. Taking the mechanistic approach as a reference, Figure 9 to 11 illustrate the uncertainty introduced by the constant-LRU approximation. For each PFT, we have taken the constant value as the regression slope of simulated COS fluxes against simulated GPP fluxes multiplied by the ratio of COS to CO_2 atmospheric concentrations. The LRU values we have thus estimated show generally lower values than the ones derived from measurements, although these cover a large range (Seibt et al., 2010; Whelan et al., 2018). It is difficult to say whether in situ and laboratory measurements are too sparse and not representative enough of the variability of plants and environmental conditions across the globe to have a reasonable confidence in their derived mean or median LRU values, or if we can use these LRU values to falsify the modelled COS and/or GPP fluxes.

28

670   Without any calibration, the mechanistic approach performs similarly to LRU approaches, when COS is transported using all known COS fluxes as inputs, and COS concentrations are evaluated at stations of the NOAA network. We have now a much finer representation of the COS fluxes as, at every timestep, the model integrates the plant's response to environmental conditions in the calculation of the internal and stomatal conductances, unlike in the LRU approach which uses constant values for each PFT.

675   In order to quantify the first order uncertainty on F_{COS} related to the fact that we have used a constant $[COS]_a$ in our implementation of the Berry model, we computed an alternative F'_{COS}, using the LRU approach based on a climatology of hemispheric monthly means of COS atmospheric concentrations (Montzka et al., 2007), the optimal LRU we derived in this study (given in Table 6), average yearly values for CO_2 atmospheric concentrations, and a climatological seasonal cycle of simulated monthly GPP per PFT. Over the 2000-2009 period, the mean

680   difference between the mean seasonal COS fluxes computed with this method (F'_{COS}) and the ones simulated with the mechanistic model (F_{COS}) amounts to -7.9% over the Northern hemisphere. As expected, the seasonal amplitude of COS fluxes is dampened as $[COS]_a$ decreases with vegetation growth. We thus have to improve our methodology to consider a varying $[COS]_a$ as was done in Berry et al. (2013), either inside the ORCHIDEE model, or as a post-processing. This requires devising some trade-off between the high frequency timestep of ORCHIDEE

685   and the cost of running the transport model. However, it is to be noted that there is no impact on the derived LRU values as the LRU does not depend on the considered $[COS]_a$, as long as the same one is considered for the computation of the COS fluxes in the mechanistic model (Eq. (3)) and for the computation of the LRU (Eq. (1)) (i.e. whether fixed or varying monthly).

However, there is currently a larger uncertainty on other COS fluxes in the global COS budget, which have an

690   important impact on simulated COS concentrations (Ma et al., 2020) and their relative seasonal changes. For example, if we use another estimation of the direct oceanic fluxes (Lennartz et al., 2017), that shows a seasonal cycle whose amplitude is comparable to the one from the vegetation in high latitudes, this results in an overestimated seasonal cycle at all sites, with the mechanistic approach having the most realistic seasonal amplitude (see Appendix C and Figure C1). An additional sensitivity test was performed to assess the impact of

695   indirect oceanic emissions via DMS oxidation on simulated seasonal cycles as the importance of these fluxes in the global COS budget is still debated (Whelan et al., 2018). Whereas the impact on northern sites is negligible, the removal of indirect oceanic emissions via the DMS of Kettle et al. (2002) decreases the seasonal amplitude of southern sites (CGO and SPO) in the same proportion in all experiments (see Appendix C and Table C2). Transport errors also add uncertainties on the simulated concentrations, especially at continental elevated sites (Remaud et

700   al., 2018). Plus, given the present discrepancies between the GPP estimates of different land surface models, it can be argued that using a mechanistic model instead of an LRU approach when comparing COS concentrations seems to be of a second order importance (Campbell et al., 2017; Hilton et al., 2017). We nevertheless note in this study that we found an uncertainty on the global vegetation COS uptake of 40% when considering three different LSMs (Launois et al., 205b), to be compared to an uncertainty of 70% when considering three LRU datasets.

705   Setting aside the uncertainty for the moment, how could we use atmospheric COS concentrations to constrain GPP? A first optimization was performed with the ORCHIDEE model in Launois et al. (2015b), who optimized a single scaling parameter applied on the vegetation COS fluxes simulated with the LRU approach, thus equivalent to a scaling factor applied on the GPP or the LRU. They assimilated the atmospheric COS concentrations measured at the NOAA air sampling stations, using the LMDz transport model (Hourdin et al., 2006) and a Bayesian

710   framework as in Kuppel et al. (2012). The optimization reduced in absolute value the estimated global vegetation

COS uptake from -1335 Gg S yr^{-1} to -708 Gg S yr^{-1}, more in line with this work's estimate based on a mechanistic

modelling of vegetation COS uptake. A mid-term perspective is to go beyond a single scaling parameter, and to

optimize a set of ORCHIDEE parameters using both atmospheric COS and CO$_2$ data. Such an approach has been

used in several studies with CO$_2$ data only (e.g. Rayner et al., 2005; Peylin et al., 2016). However, compared to

715   CO$_2$, the spatial coverage of COS surface observations is still too sparse to accurately constrain the GPP and

therefore ORCHIDEE parameters (Ma et al., 2020). There is some hope that new satellite retrievals of COS column

content, such as with the IASI (Infrared Atmospheric Sounder Interferometer) instrument, could have enough

accuracy to better constrain the surface fluxes (Serio et al., 2020).

5 Conclusions and Outlooks

720   We have implemented inside the ORCHIDEE land surface model the mechanistic model of Berry et al. (2013) for

COS uptake by the continental vegetation. We further adapted the ORCHIDEEE model to compute the stomatal

conductance in the absence of photosynthesis. Modelled COS fluxes were compared at site scale against

measurements at the Harvard temperate deciduous broadleaf forest (USA) and at the Hyytiälä Scots pine forest

(Finland), yielding relative RMSDs of 35 and 36% for the diel cycle respectively, and of 44 and 25% for the

725   seasonal cycle. Parameters could be optimized to get a better agreement. The model notably reproduced expected

observed behaviours such as the relationship between LRU and PAR depicted in Kooijmans et al. (2019), the

proportion of COS nighttime fluxes, as well as the dominant effect of the internal conductance during low spring

temperatures, and at daytime.

Our global estimate of COS uptake by continental vegetation of -756 Gg S yr^{-1} is in the lower range of former

730   studies. From our modelled COS and GPP fluxes, we derived optimal LRU values per PFT and compared them to

values derived from experiments. We found lower LRU values than those observed for C3 species and intermediate

ones for C4 species, evidencing the crucial role of the α parameter in the Berry model, linking the COS internal

conductance to the photosynthetic capacity, and the need for more site measurements of COS fluxes to better

constrain its values.

735   We transported the COS fluxes from the mechanistic and LRU approaches using the LMDz6 model. We evaluated

the modelled COS atmospheric concentrations against observations at stations of the NOAA network and found

comparable results for both approaches.

As a general conclusion and for the moment, we can say that the mechanistic model is particularly valuable when

studying small time or spatial scales using COS fluxes, while for global analyses using COS concentrations, both

740   the mechanistic and LRU approaches give similar results.

The fact that the global COS budget has so many components with a large uncertainty (Whelan et al., 2018) limits

the use of COS concentrations as a constraint for GPP in land surface models on the global scale, for the present

time. Our next step will be to refine the estimation for COS soil fluxes and to implement inside ORCHIDEE a

mechanistic model for soil COS fluxes (Ogée et al., 2016; Sun et al., 2015). Having both the vegetation and soil

745   contributions, we will also be able to assimilate ecosystem COS fluxes to optimize COS-related parameters such

as α in the internal conductance formulation from the Berry et al. (2013) model for vegetation uptake, and those

related to the stomatal conductance (Wehr et al., 2017; Berkelhammer et al., 2020). We will also later look at the

complementary constraints on GPP brought by COS and Solar-Induced Fluorescence, another GPP proxy (Bacour et al., 2019; Whelan et al., 2020).

750 **Appendices**

Appendix A. Tables for modelled boundary conductances and minimum stomatal conductances
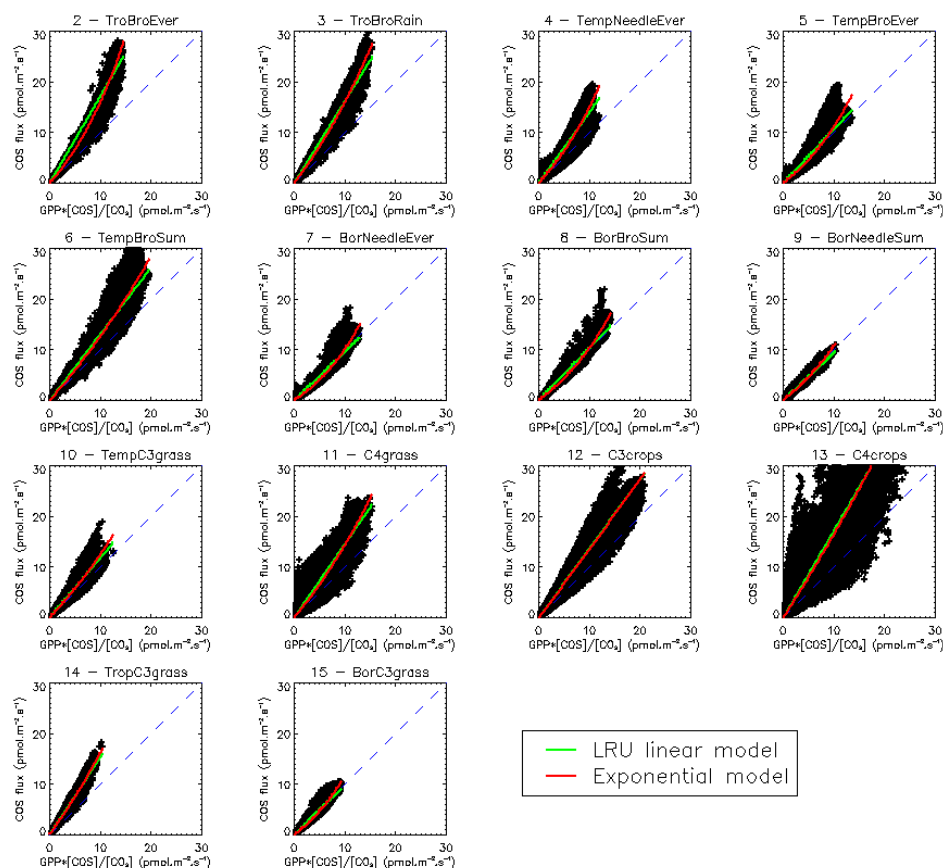
Table A1: Ratios of modelled boundary conductance to stomatal conductance and internal conductance, respectively, at the two studied sites, computed over year 2012 at Harvard Forest and 2017 at Hyytiälä

Ratio	Harvard Forest		Hyytiälä	
	Boundary to stomatal	Boundary to internal	Boundary to stomatal	Boundary to internal
Median	**72**	**37**	**56**	**48**
Minimum	2	3	95	4
Maximum	2239	4555	3	1801

755 **Table A2: Minimum stomatal conductance to CO₂ (mmol m⁻² s⁻¹) for each PFT in Lombardozzi et al. (2017) and ORCHIDEE. No value is given for C4 crops in Lombardozzi et al. (2017).**

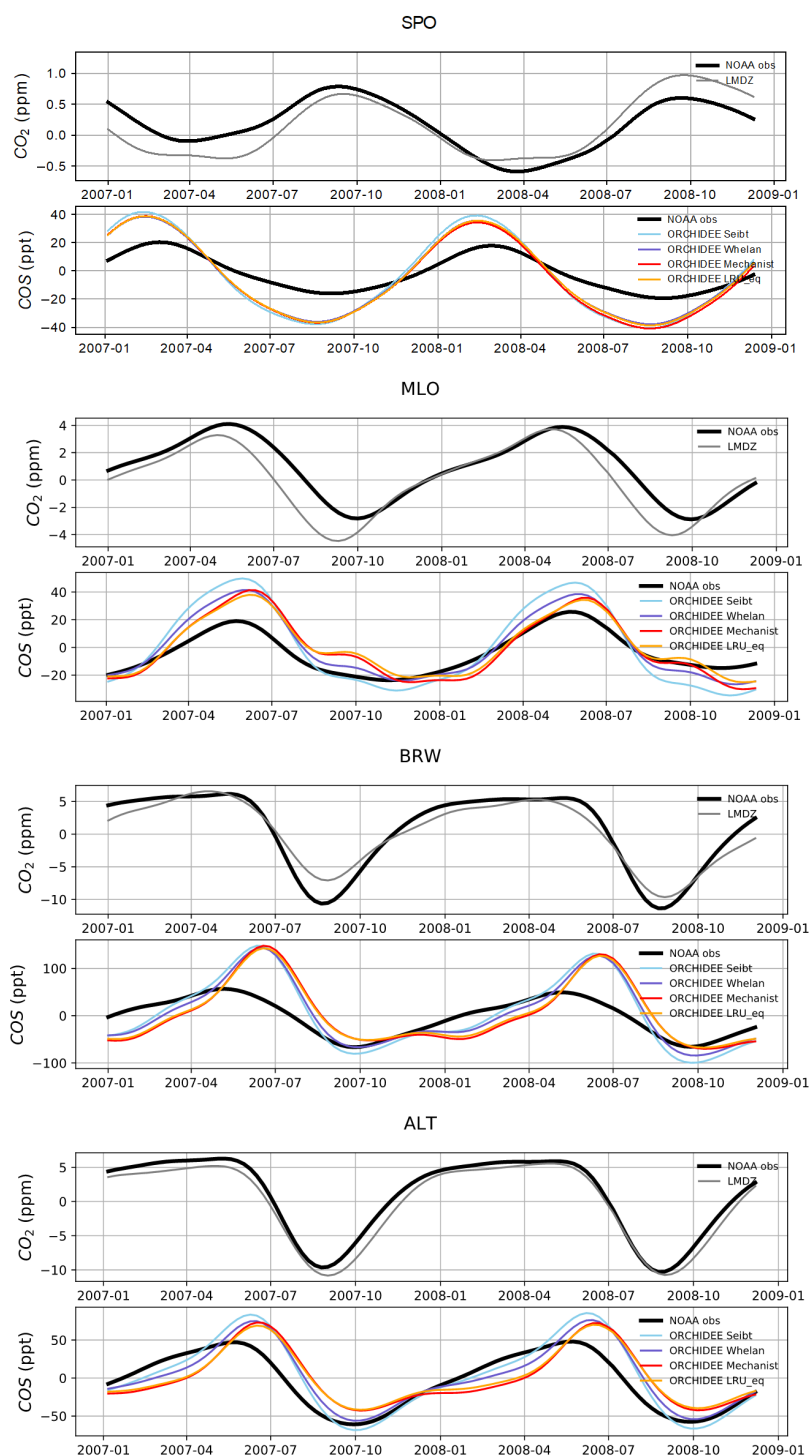|	Mean minimum conductance in Lombardozzi et al. (2017)	Minimum conductance in ORCHIDEE
1 - Bare soil	0	0
2 - Tropical Broad-leaved Evergreen Forest	90.488	6.25
3 - Tropical Broad-leaved Raingreen Forest	109.744	6.25
4 - Temperate Needleleaf Evergreen Forest	16.896	6.25
5 - Temperate Broad-leaved Evergreen Forest	34.017	6.25
6 - Temperate Broad-leaved Summergreen Forest	72.637	6.25
7 - Boreal Needleleaf Evergreen Forest	8	6.25
8 - Boreal Broad-leaved Summergreen Forest	50	6.25
9 - Boreal Needleleaf Summergreen Forest	29	6.25
10 - C3 Grass	157.988	6.25
11 - C4 Grass	93.933	18.75
12 - C3 Agriculture	60.629	6.25
13 - C4 Agriculture	x	18.75

Appendix B. Exponential fit for LRU

Figure B1: Scatterplots of COS fluxes against GPP multiplied by the ratio of COS to CO2 concentrations, using a climatology of monthly fluxes over the 2000-2009 period and yearly global averages for CO_2 concentrations and a fixed value of 500 ppt for the COS concentration. Each subplot represents one of the 14 vegetated PFTs used in ORCHIDEE. The LRU model in green represents the linear regression, while the exponential model (see text) is represented in red. The blue dashes lines show the 1:1 line.

Appendix C. Sensitivity tests for the modelling of atmospheric COS concentrations

C1. Simulating COS atmospheric concentration at stations: impact of the oceanic emissions

We performed the same experiment as in Sect. 3.4, except that the oceanic fluxes (direct and indirect) are here from Lennartz et al. (2017). In our case, the oceanic emissions (in particular direct oceanic emissions) have more impact than the LRU on the seasonality at surface sites from the NOAA network.

Figure C1: Detrended temporal evolutions of simulated and observed CO_2 and COS concentrations at four selected sites, for the mechanistic (ORCHIDEE Mechanist) and LRU approaches (ORCHIDEE Seibt, ORCHIDEE Whelan, ORCHIDEE LRU_eq), simulated with LMDz6 transport between 2007 and 2009. The ORCHIDEE LRU_eq line
775 **(orange) corresponds to the concentrations simulated using the optimal equivalent LRU derived from the mechanistic model. The curves have been detrended beforehand and filtered to remove the synoptic variability (see Sect. 2.2.4).**

Table C1: Prescribed COS surface fluxes used as model input. Mean magnitudes of different types of fluxes are given for the period 2000-2009

Type of COS flux	Temporal resolution	Total (Gg S yr^{-1})	Data Source
Anthropogenic	Monthly, interannual	337.3	Zumkehr et al. (2018)
Biomass burning	Monthly, interannual	56.3	Stinecipher et al. (2019)
Soil	Monthly, climatological	-409.0	Launois et al. (2015b)
Ocean	Monthly, climatological	344.0	Lennartz et al. (2017)
Vegetation uptake	Monthly, interannual		This work, including mechanistic and LRU approaches (Seibt et al., 2010; Whelan et al., 2018).

780 **C2. DMS sensitivity study**

We further tested the impact of the indirect COS fluxes through DMS on the simulated concentrations at NOAA sites. To do that, we compared the atmospheric concentrations given with and without prescribing indirect oceanic fluxes through DMS using the Launois et al. (2015a) oceanic fluxes. In our case, the removal of the DMS oceanic emissions decreases the seasonal amplitude at SPO and CGO but have very few impacts at other sites. We also

785 performed the same experiment using the Sinikka et al. (2017) fluxes and reported no impact of DMS indirect fluxes on simulated concentrations at NOAA sites.

Table C2: Normalized standard deviations (NSDs) of the simulated concentrations by the observed concentrations. Within brackets are the Pearson correlation coefficients (R) between simulated and observed COS concentrations for the mechanistic approach including the DMS or not, calculated between 2004 and 2009 at 10 NOAA stations.

	SPO	CGO	SMO	KUM	MLO	NWR	LEF	MHD	BRW	ALT
ORCHIDEE Mechanist (DMS)	1.10 (0.97)	1.01 (0.97)	0.35 (0.4)	0.90 (0.95)	1.05 (0.92)	1.26 (0.63)	1.34 (0.94)	1.09 (0.85)	0.69 (0.91)	0.64 (0.96)
ORCHIDEE Mechanist (Without DMS)	*0.74* (0.91)	*0.53* (0.94)	0.38 (0.20)	0.90 (0.95)	1.04 (0.91)	1.31 (0.64)	1.40 (0.94)	0.93 (0.94)	0.74 (0.90)	0.65 (0.96)

790 **Code availability**

The ORCHIDE model is available on request to the authors.

Author contribution

FM and PP devised the research. CA and FM coded the ORCHIDEE developments and made the simulations. MR and PP dealt with the transport model. LMJK and KMK provided the Hyytiälä data. RC and RW provided the Harvard Forest data. JEC, SB, SAM, NR, US, YPS, NV, MEW were consulted on their respective expertise. FM, CA and MR analysed the results and wrote the first draft. All authors contributed to the manuscript.

Competing interests

The authors declare that they have no conflict of interest.

Acknowledgments

References

Allen, M., Babiker, M., Chen, Y., Taylor, M., Tschakert Australia, P., Waisman, H., Warren, R., Zhai, P., Zickfeld, K., Zhai, P., Pörtner, H., Roberts, D., Skea, J., Shukla, P., Pirani, A., Moufouma-Okia, W., Péan, C., Pidcock, R., Connors, S., Matthews, J., Chen, Y., Zhou, X., Gomis, M., Lonnoy, E., Maycock, T., Tignor, M. and Waterfield, T.: IPCCC 1.5C: Summary for Policymakers, Aromar Revi [online] Available from: https://www.ipcc.ch/site/assets/uploads/sites/2/2019/05/SR15_SPM_version_report_LR.pdf, 2018.

Anav, A., Friedlingstein, P., Beer, C., Ciais, P., Harper, A., Jones, C., Murray-Tortarolo, G., Papale, D., Parazoo, N. C., Peylin, P., Piao, S., Sitch, S., Viovy, N., Wiltshire, A. and Zhao, M.: Spatiotemporal patterns of terrestrial gross primary production: A review, Rev. Geophys., 53(3), 785–818, doi:10.1002/2015RG000483, 2015.

Badger, M. R. and Price, G. D.: CO_2 concentrating mechanisms in cyanobacteria: Molecular components, their diversity and evolution, J. Exp. Bot., doi:10.1093/jxb/erg076, 2003.

Bacour, C., Maignan, F., MacBean, N., Porcar-Castell, A., Flexas, J., Frankenberg, C., Peylin, P., Chevallier, F., Vuichard, N. and Bastrikov, V.: Improving Estimates of Gross Primary Productivity by Assimilating Solar-Induced Fluorescence Satellite Retrievals in a Terrestrial Biosphere Model Using a Process-Based SIF Model, J. Geophys. Res. Biogeosciences, 124(11), 3281–3306, doi:10.1029/2019JG005040, 2019.

Ball, J. T., Woodrow, I. E. and Berry, J. A.: A Model Predicting Stomatal Conductance and its Contribution to the Control of Photosynthesis under Different Environmental Conditions, in Progress in Photosynthesis Research, pp. 221–224, Springer Netherlands., 1987.Barkley, M. P., Palmer, P. I., Boone, C. D., Bernath, P. F. and Suntharalingam, P.: Global distributions of carbonyl sulfide in the upper troposphere and stratosphere, Geophys. Res. Lett., 35(14), 2008.

Berkelhammer, M., Alsip, B., Matamala, R., Cook, D., Whelan, M. E., Joo, E., Bernacchi, C., Miller, J. and Meyers, T.: Seasonal Evolution of Canopy Stomatal Conductance for a Prairie and Maize Field in the Midwestern United States from Continuous Carbonyl Sulfide Fluxes, Geophys. Res. Lett., 47(6), doi:10.1029/2019GL085652, 2020.

835 Berry, J., Wolf, A., Campbell, J. E., Baker, I., Blake, N., Blake, D., Denning, a. S., Kawa, S. R., Montzka, S. a., Seibt, U., Stimler, K., Yakir, D. and Zhu, Z.: A coupled model of the global cycles of carbonyl sulfide and CO_2: A possible new window on the carbon cycle, J. Geophys. Res. Biogeosciences, 118(2), 842–852, doi:10.1002/jgrg.20068, 2013.

Bloom, A. A., Exbrayat, J. F., Van Der Velde, I. R., Feng, L. and Williams, M.: The decadal state of the terrestrial
840 carbon cycle: Global retrievals of terrestrial carbon allocation, pools, and residence times, Proc. Natl. Acad. Sci. U. S. A., 113(5), 1285–1290, doi:10.1073/pnas.1515160113, 2016.

Botta, A., Viovy, N., Ciais, P., Friedlingstein, P. and Monfray, P.: A global prognostic scheme of leaf onset using satellite data, Glob. Chang. Biol., 6(7), 709–725, doi:10.1046/j.1365-2486.2000.00362.x, 2000.

Caird, M. A., Richards, J. H. and Donovan, L. A.: Nighttime stomatal conductance and transpiration in C3 and C4
845 plants, Plant Physiol., 143(1), 4–10, doi:10.1104/pp.106.092940, 2007.

Campbell, J. E., Carmichael, G. R., Chai, T., Mena-Carrasco, M., Tang, Y., Blake, D. R., Blake, N. J., Vay, S. A., Collatz, G. J., Baker, I., Berry, J. A., Montzka, S. A., Sweeney, C., Schnoor, J. L. and Stanier, C. O.: Photosynthetic Control of Atmospheric Carbonyl Sulfide During the Growing Season, Science (80-.)., 322(5904), 1085–1088, doi:10.1126/science.1164015, 2008.

850 Campbell, J. E., Berry, J. A., Seibt, U., Smith, S. J., Montzka, S. A., Launois, T., Belviso, S., Bopp, L. and Laine, M.: Large historical growth in global terrestrial gross primary production, Nature, 544(7648), 84–87, doi:10.1038/nature22030, 2017.

Ciais, P., Sabine, C., Bala, G., Bopp, L., Brovkin, V., Canadell, J., Chhabra, A., DeFries, R., Galloway, J., Heimann, M., Jones, C., Quéré, C. Le, Myneni, R. B., Piao, S. and P. Thornton: Carbon and other
855 biogeochemical cycles. In Climate Change 2013 the Physical Science Basis: Working Group I Contribution to the Fifth Assessment Report of the Intergovernmental Panel on Climate Change, 465–570. doi:10.10, Clim. Chang. 2013 Phys. Sci. Basis Work. Gr. I Contrib. to Fifth Assess. Rep. Intergov. Panel Clim. Chang., 9781107057, 465–570, doi:10.1017/CBO9781107415324.015, 2013.

Collatz, G., Ribas-Carbo, M. and Berry, J.: Coupled Photosynthesis-Stomatal Conductance Model for Leaves of
860 C4 Plants, Funct. Plant Biol., doi:10.1071/pp9920519, 1992.

Commane, R., Lindaas, J., Benmergui, J., Luus, K. A., Chang, R. Y. W., Daube, B. C., Euskirchen, E. S., Henderson, J. M., Karion, A., Miller, J. B., Miller, S. M., Parazoo, N. C., Randerson, J. T., Sweeney, C., Tans, P., Thoning, K., Veraverbeke, S., Miller, C. E. and Wofsy, S. C.: Carbon dioxide sources from Alaska driven by increasing early winter respiration from Arctic tundra, Proc. Natl. Acad. Sci. U. S. A.,
865 114(21), 5361–5366, doi:10.1073/pnas.1618567114, 2017.

Commane, R., Meredith, L. K., Baker, I. T., Berry, J. A., Munger, J. W., Montzka, S. A., Templer, P. H., Juice, S. M., Zahniser, M. S. and Wofsy, S. C.: Seasonal fluxes of carbonyl sulfide in a midlatitude forest, Proc. Natl. Acad. Sci. U. S. A., 112(46), 14162–14167, doi:10.1073/pnas.1504131112, 2015.

Conway, T. J., Tans, P. P., Waterman, L. S.: Atmospheric CO_2 records from sites in the NOAA/CMDL air
870 sampling network. In T. A. Boden, D. P. Kaiser, R. J. Sepanski, 14 F. W. Stoss (eds.), Trends '93: A Compendium of Data on Global Change. CDIAC, Oak Ridge National Laboratory, Oak Ridge, Tenn, 41-119, 1994.

de Rosnay, P. and Polcher, J.: Modelling root water uptake in a complex land surface scheme coupled to a GCM, Hydrol. Earth Syst. Sci., 2(2/3), 239–255, doi:10.5194/hess-2-239-1998, 1998.

875 Dufresne, J. L., Foujols, M. A., Denvil, S., Caubel, A., Marti, O., Aumont, O., Balkanski, Y., Bekki, S., Bellenger, H., Benshila, R., Bony, S., Bopp, L., Braconnot, P., Brockmann, P., Cadule, P., Cheruy, F., Codron, F., Cozic, A., Cugnet, D., de Noblet, N., Duvel, J. P., Ethé, C., Fairhead, L., Fichefet, T., Flavoni, S., Friedlingstein, P., Grandpeix, J. Y., Guez, L., Guilyardi, E., Hauglustaine, D., Hourdin, F., Idelkadi, A., Ghattas, J., Joussaume, S., Kageyama, M., Krinner, G., Labetoulle, S., Lahellec, A., Lefebvre, M. P.,
880 Lefevre, F., Levy, C., Li, Z. X., Lloyd, J., Lott, F., Madec, G., Mancip, M., Marchand, M., Masson, S., Meurdesoif, Y., Mignot, J., Musat, I., Parouty, S., Polcher, J., Rio, C., Schulz, M., Swingedouw, D., Szopa, S., Talandier, C., Terray, P., Viovy, N. and Vuichard, N.: Climate change projections using the

IPSL-CM5 Earth System Model: From CMIP3 to CMIP5, Clim. Dyn., doi:10.1007/s00382-012-1636-1, 2013.

885   Evans, J. R., von Caemmerer, S., Setchell, B. A. and Hudson, G. S.: The relationship between CO_2 transfer conductance and leaf anatomy in transgenic tobacco with a reduced content of Rubisco, Aust. J. Plant Physiol., doi:10.1071/PP9940475, 1994.

Farquhar, G. D., Lloyd, J., Taylor, J. A., Flanagan, L. B., Syvertsen, J. P., Hubick, K. T., Wong, S. C. and Ehleringer, J. R.: Vegetation effects on the isotope composition of oxygen in atmospheric CO2, Nature,
890   363(6428), 439–443, doi:10.1038/363439a0, 1993.

Farquhar, G. D., von Caemmerer, S. and Berry, J. A.: A biochemical model of photosynthetic CO_2 assimilation in leaves of C3 species, Planta, 149(1), 78–90, doi:10.1007/BF00386231, 1980.

Folberth, G. A., Hauglustaine, D. A., Lathièrel, J. and Brocheton, F.: Interactive chemistry in the Laboratoire de Météorologie Dynamique general circulation model: Model description and impact analysis of biogenic
895   hydrocarbons on tropospheric chemistry, Atmos. Chem. Phys., doi:10.5194/acp-6-2273-2006, 2006.

Friedlingstein, P., Jones, M. W., O'Sullivan, M., Andrew, R. M., Hauck, J., Peters, G. P., Peters, W., Pongratz, J., Sitch, S., Le Quéré, C., DBakker, O. C. E., Canadell1, J. G., Ciais1, P., Jackson, R. B., Anthoni1, P., Barbero, L., Bastos, A., Bastrikov, V., Becker, M., Bopp, L., Buitenhuis, E., Chandra, N., Chevallier, F., Chini, L. P., Currie, K. I., Feely, R. A., Gehlen, M., Gilfillan, D., Gkritzalis, T., Goll, D. S., Gruber,
900   N., Gutekunst, S., Harris, I., Haverd, V., Houghton, R. A., Hurtt, G., Ilyina, T., Jain, A. K., Joetzjer, E., Kaplan, J. O., Kato, E., Goldewijk, K. K., Korsbakken, J. I., Landschützer, P., Lauvset, S. K., Lefèvre, N., Lenton, A., Lienert, S., Lombardozzi, D., Marland, G., McGuire, P. C., Melton, J. R., Metzl, N., Munro, D. R., Nabel, J. E. M. S., Nakaoka, S. I., Neill, C., Omar, A. M., Ono, T., Peregon, A., Pierrot, D., Poulter, B., Rehder, G., Resplandy, L., Robertson, E., Rödenbeck, C., Séférian, R., Schwinger, J.,
905   Smith, N., Tans, P. P., Tian, H., Tilbrook, B., Tubiello, F. N., Van Der Werf, G. R., Wiltshire, A. J. and Zaehle, S.: Global carbon budget 2019, Earth Syst. Sci. Data, 11(4), 1783–1838, doi:10.5194/essd-11-1783-2019, 2019.

Friend, A. D., Arneth, A., Kiang, N. Y., Lomas, M., Ogée, J., Rödenbeck, C., Running, S. W., Santaren, J. D., Sitch, S., Viovy, N., Ian Woodward, F. and Zaehle, S.: FLUXNET and modelling the global carbon
910   cycle, Glob. Chang. Biol., 13(3), 610–633, doi:10.1111/j.1365-2486.2006.01223.x, 2007.

Goldan, P. D., Fall, R., Kuster, W. C., and Fehsenfeld, F. C.: Uptake of COS by growing vegetation: A major tropospheric sink, J. Geophys. Res.-Atmos., 93, 14186–14192, https://doi.org/10.1029/JD093iD11p14186, 1988.

Graven, H. D., Keeling, R. F., Piper, S. C., Patra, P. K., Stephens, B. B., Wofsy, S. C., Welp, L. R., Sweeney, C.,
915   Tans, P. P., Kelley, J. J., Daube, B. C., Kort, E. A., Santoni, G. W. and Bent, J. D.: Enhanced seasonal exchange of CO_2 by Northern ecosystems since 1960, Science (80-.)., 341(6150), 1085–1089, doi:10.1126/science.1239207, 2013.

Hauglustaine, D. A., Hourdin, F., Jourdain, L., Filiberti, M. A., Walters, S., Lamarque, J. F. and Holland, E. A.: Interactive chemistry in the Laboratoire de Météorologie Dynamique general circulation model:
920   Description and background tropospheric chemistry evaluation, J. Geophys. Res. D Atmos., doi:10.1029/2003jd003957, 2004.

Hauglustaine, D. A., Balkanski, Y. and Schulz, M.: A global model simulation of present and future nitrate aerosols and their direct radiative forcing of climate, Atmos. Chem. Phys., doi:10.5194/acp-14-11031-2014, 2014.

925   Hilton, T. W., Whelan, M. E., Zumkehr, A., Kulkarni, S., Berry, J. A., Baker, I. T., Montzka, S. A., Sweeney, C., Miller, B. R. and Elliott Campbell, J.: Peak growing season gross uptake of carbon in North America is largest in the Midwest USA, Nat. Clim. Chang., 7(6), 450–454, doi:10.1038/nclimate3272, 2017.

Hilton, T. W., Zumkehr, A., Kulkarni, S., Berry, J., Whelan, M. E. and Elliott Campbell, J.: Large variability in ecosystem models explains uncertainty in a critical parameter for quantifying GPP with carbonyl
930   sulphide, Tellus, Ser. B Chem. Phys. Meteorol., 67(1), doi:10.3402/tellusb.v67.26329, 2015.

Hourdin, F. and Talagrand, O.: Eulerian backtracking of atmospheric tracers. I: Adjoint derivation and parametrization of subgrid-scale transport, Q. J. R. Meteorol. Soc., 132(615), 567–583, doi:10.1256/qj.03.198.A, 2006.

Hourdin, F., Talagrand, O. and Idelkadi, A.: Eulerian backtracking of atmospheric tracers. II: Numerical aspects,
935   Q. J. R. Meteorol. Soc., doi:10.1256/qj.03.198.B, 2006.

IPCC: IPCC Special Report on Climate Change, Desertification, Land Degradation, Sustainable Land Management, Food Security, and Greenhouse gas fluxes in Terrestrial Ecosystems, Summ. Policymakers Approv. Draft, 74–102, doi:10.4337/9781784710644, 2019a.

IPCC: IPCC Special Report on the Ocean and Cryosphere in a Changing Climate, in IPCC Summary for Policymalers., 2019b.

940

Joiner, J., Yoshida, Y., Zhang, Y., Duveiller, G., Jung, M., Lyapustin, A., Wang, Y. and Tucker, C.: Estimation of Terrestrial Global Gross Primary Production (GPP) with Satellite Data-Driven Models and Eddy Covariance Flux Data, Remote Sens., 10(9), 1346, doi:10.3390/rs10091346, 2018.

Kattge, J. and Knorr, W.: Temperature acclimation in a biochemical model of photosynthesis: A reanalysis of data from 36 species, Plant, Cell Environ., 30(9), 1176–1190, doi:10.1111/j.1365-3040.2007.01690.x, 2007.

945

Kettle, A. J., Kuhn, U., Von Hobe, M., Kesselmeier, J. and Andreae, M. O.: Global budget of atmospheric carbonyl sulfide: Temporal and spatial variations of the dominant sources and sinks, J. Geophys. Res. Atmos., 107(22), ACH 25-1, doi:10.1029/2002JD002187, 2002.

Kohonen, K.-M., Kolari, P., Kooijmans, L. M. J., Chen, H., Seibt, U., Sun, W. and Mammarella, I.: Towards standardized processing of eddy covariance flux measurements of carbonyl sulfide, Atmos. Meas. Tech., 13(7), 3957–3975, doi:10.5194/amt-13-3957-2020, 2020.

950

Kooijmans, L. M. J., Uitslag, N. A. M., Zahniser, M. S., Nelson, D. D., Montzka, S. A., and Chen, H.: Continuous and high-precision atmospheric concentration measurements of COS, CO_2, CO and H_2O using a quantum cascade laser spectrometer (QCLS), Atmos. Meas. Tech., 9, 5293–5314, https://doi.org/10.5194/amt-9-5293-2016, 2016.

955

Kooijmans, L. M. J., Maseyk, K., Seibt, U., Sun, W., Vesala, T., Mammarella, I., Kolari, P., Aalto, J., Franchin, A., Vecchi, R., Valli, G. and Chen, H.: Canopy uptake dominates nighttime carbonyl sulfide fluxes in a boreal forest, Atmos. Chem. Phys., 17(18), 11453–11465, doi:10.5194/acp-17-11453-2017, 2017.

Kooijmans, L. M. J., Sun, W., Aalto, J., Erkkilä, K. M., Maseyk, K., Seibt, U., Vesala, T., Mammarella, I. and Chen, H.: Influences of light and humidity on carbonyl sulfide-based estimates of photosynthesis, Proc. Natl. Acad. Sci. U. S. A., 116(7), 2470–2475, doi:10.1073/pnas.1807600116, 2019.

960

Kuppel, S., Peylin, P., Chevallier, F., Bacour, C., Maignan, F. and Richardson, A. D.: Constraining a global ecosystem model with multi-site eddy-covariance data, Biogeosciences, 9(10), 3757–3776, doi:10.5194/bg-9-3757-2012, 2012.

965

Kuppel, S., Peylin, P., Maignan, F., Chevallier, F., Kiely, G., Montagnani, L. and Cescatti, A.: Model-data fusion across ecosystems: From multisite optimizations to global simulations, Geosci. Model Dev., 7(6), 2581–2597, doi:10.5194/gmd-7-2581-2014, 2014.

Lardy, R., Bellocchi, G. and Soussana, J.: Environmental Modelling & Software Short communication A new method to determine soil organic carbon equilibrium, Environ. Model. Softw., 26(12), 1759–1763, doi:10.1016/j.envsoft.2011.05.016, 2011.

970

Landschützer, P., Gruber, N. and Bakker, D. C. E.: A 30 years observation-based global monthly gridded sea surface pCO_2 product from 1982 through 2011 (NCEI Accession 0160558). Version 2.2, NOAA Natl. Centers Environ. Inf., doi:10.3334/cdiac/otg.spco2_1982_2011_eth_somffn, 2015.

Launois, T., Belviso, S., Bopp, L., Fichot, C. G. and Peylin, P.: A new model for the global biogeochemical cycle of carbonyl sulfide – Part 1: Assessment of direct marine emissions with an oceanic general circulation and biogeochemistry model, Atmos. Chem. Phys., 15(5), 2295–2312, doi:10.5194/acp-15-2295-2015, 2015a.

975

Launois, T., Peylin, P., Belviso, S. and Poulter, B.: A new model of the global biogeochemical cycle of carbonyl sulfide – Part 2: Use of carbonyl sulfide to constrain gross primary productivity in current vegetation models, Atmos. Chem. Phys., 15(16), 9285–9312, doi:10.5194/acp-15-9285-2015, 2015b.

980

Le Quéré, C., Andrew, R., Friedlingstein, P., Sitch, S., Hauck, J., Pongratz, J., Pickers, P., Ivar Korsbakken, J., Peters, G., Canadell, J., Arneth, A., Arora, V., Barbero, L., Bastos, A., Bopp, L., Ciais, P., Chini, L., Ciais, P., Doney, S., Gkritzalis, T., Goll, D., Harris, I., Haverd, V., Hoffman, F., Hoppema, M., Houghton, R., Hurtt, G., Ilyina, T., Jain, A., Johannessen, T., Jones, C., Kato, E., Keeling, R., Klein Goldewijk, K., Landschützer, P., Lefèvre, N., Lienert, S., Liu, Z., Lombardozzi, D., Metzl, N., Munro, D., Nabel, J., Nakaoka, S. I., Neill, C., Olsen, A., Ono, T., Patra, P., Peregon, A., Peters, W., Peylin, P., Pfeil, B., Pierrot, D., Poulter, B., Rehder, G., Resplandy, L., Robertson, E., Rocher, M., Rödenbeck, C., Schuster, U., Skjelvan, I., Séférian, R., Skjelvan, I., Steinhoff, T., Sutton, A., Tans, P., Tian, H.,

985

990   Tilbrook, B., Tubiello, F., Van Der Laan-Luijkx, I., Van Der Werf, G., Viovy, N., Walker, A., Wiltshire, A., Wright, R., Zaehle, S. and Zheng, B.: Global Carbon Budget 2018, Earth Syst. Sci. Data, 10(4), 2141–2194, doi:10.5194/essd-10-2141-2018, 2018.

Lennartz, S. T., Marandino, C. A., von Hobe, M., Cortes, P., Quack, B., Simo, R., Booge, D., Pozzer, A., Steinhoff, T., Arevalo-Martinez, D. L., Kloss, C., Bracher, A., Röttgers, R., Atlas, E. and Krüger, K.: Direct oceanic emissions unlikely to account for the missing source of atmospheric carbonyl sulfide, Atmos.
995   Chem. Phys., 17(1), 385–402, doi:10.5194/acp-17-385-2017, 2017.

Lombardozzi, D. L., Zeppel, M. J. B., Fisher, R. A. and Tawfik, A.: Representing nighttime and minimum conductance in CLM4.5: Global hydrology and carbon sensitivity analysis using observational constraints, Geosci. Model Dev., 10(1), 321–331, doi:10.5194/gmd-10-321-2017, 2017.

Ma, J., Kooijmans, L. M. J., Cho, A., Montzka, S. A., Glatthor, N., Worden, J. R., Kuai, L., Atlas, E. L., and Krol,
1000   M. C.: Inverse modelling of carbonyl sulfide: implementation, evaluation and implications for the global budget, Atmos. Chem. Phys. Discuss., https://doi.org/10.5194/acp-2020-603, in review, 2020.

MacBean, N., Maignan, F., Peylin, P., Bacour, C., Bréon, F.-M. and Ciais, P.: Using satellite data to improve the leaf phenology of a global terrestrial biosphere model, Biogeosciences, 12(23), 7185–7208, doi:10.5194/bg-12-7185-2015, 2015.

1005   Maseyk, K., Berry, J. A., Billesbach, D., Campbell, J. E., Torn, M. S., Zahniser, M. and Seibt, U.: Sources and sinks of carbonyl sulfide in an agricultural field in the Southern Great Plains, Proc. Natl. Acad. Sci. U. S. A., 111(25), 9064–9069, doi:10.1073/pnas.1319132111, 2014.

Montzka, S. A., Calvert, P., Hall, B. D., Elkins, J. W., Conway, T. J., Tans, P. P. and Sweeney, C. S.: On the global distribution, seasonality, and budget of atmospheric carbonyl sulfide (COS) and some similarities to
1010 CO_2, J. Geophys. Res. Atmos., 112(9), 1–15, doi:10.1029/2006JD007665, 2007.

Norton, A. J., Rayner, P. J., Koffi, E. N., Scholze, M., Silver, J. D. and Wang, Y.-P.: Estimating global gross primary productivity using chlorophyll fluorescence and a data assimilation system with the BETHY-SCOPE model, Biogeosciences, 16(15), 3069–3093, doi:10.5194/bg-16-3069-2019, 2019.Notni, J., Schenk, S., Protoschill-Krebs, G., Kesselmeier, J., and Anders, E.: The missing link in COS
1015   metabolism: a model study on the reactivation of carbonic anhydrase from its hydrosulfide analogue, ChemBioChem, 8, 530–536, https://doi.org/10.1002/cbic.200600436, 2007.

Ogawa, T., Noguchi, K., Saito, M., Nagahata, Y., Kato, H., Ohtaki, A., Nakayama, H., Dohmae, N., Matsushita, Y., Odaka, M., Yohda, M., Nyunoya, H., and Katayama, Y.: Carbonyl sulfide hydrolase from Thiobacillus thioparus strain THI115 is one of the β-carbonic anhydrase family enzymes, J. Am. Chem.
1020   Soc., 135, 3818–3825, https://doi.org/10.1021/ja307735e, 2013.

Ogée, J., Sauze, J., Kesselmeier, J., Genty, B., Van Diest, H., Launois, T. and Wingate, L.: A new mechanistic framework to predict OCS fluxes from soils, Biogeosciences, 13(8), 2221–2240, doi:10.5194/bg-13-2221-2016, 2016.

Parazoo, N. C., Denning, A. S., Berry, J. A., Wolf, A., Randall, D. A., Kawa, S. R., Pauluis, O. and Doney, S. C.:
1025   Moist synoptic transport of CO_2 along the mid-latitude storm track, Geophys. Res. Lett., 38(9), n/a-n/a, doi:10.1029/2011GL047238, 2011.

Peters, W., van der Velde, I. R., van Schaik, E., Miller, J. B., Ciais, P., Duarte, H. F., van der Laan-Luijkx, I. T., van der Molen, M. K., Scholze, M., Schaefer, K., Vidale, P. L., Verhoef, A., Wårlind, D., Zhu, D., Tans, P. P., Vaughn, B. and White, J. W. C.: Increased water-use efficiency and reduced CO_2 uptake by plants
1030   during droughts at a continental scale, Nat. Geosci., 11(10), 744–748, doi:10.1038/s41561-018-0212-7, 2018.

Peylin, P. et al.: The ORCHIDEE global land surface model version v2.0: description and evaluation, *in prep*.

Peylin, P., Ciais, P., Denning, A. S., Tans, P. P., Berry, J. A. and White, J. W. C.: A 3-dimensional study of $\delta^{18}O$ in atmospheric CO_2: Contribution of different land ecosystems, Tellus, Ser. B Chem. Phys. Meteorol.,
1035   51(3), 642–667, doi:10.3402/tellusb.v51i3.16452, 1999.

Phillips, N. G., Lewis, J. D., Logan, B. A. and Tissue, D. T.: Inter- and intra-specific variation in nocturnal water transport in Eucalyptus, Tree Physiol., 30(5), 586–596, doi:10.1093/treephys/tpq009, 2010.

Poulter, B., MacBean, N., Hartley, A., Khlystova, I., Arino, O., Betts, R., Bontemps, S., Boettcher, M., Brockmann, C., Defourny, P., Hagemann, S., Herold, M., Kirches, G., Lamarche, C., Lederer, D., Ottlé,
1040   C., Peters, M. and Peylin, P.: Plant functional type classification for earth system models: Results from

the European Space Agency's Land Cover Climate Change Initiative, Geosci. Model Dev., 8(7), 2315–2328, doi:10.5194/gmd-8-2315-2015, 2015.

Protoschill-Krebs, G., Wilhelm, C., and Kesselmeier, J.: Consumption of carbonyl sulphide (COS) by higher plant carbonic anhydrase (CA), Atmos. Environ., 30, 3151–3156, https://doi.org/10.1016/1352-2310(96)00026-X, 1996.

Rayner, P. J., Scholze, M., Knorr, W., Kaminski, T., Giering, R. and Widmann, H.: Two decades of terrestrial carbon fluxes from a carbon cycle data assimilation system (CCDAS), Global Biogeochem. Cycles, 19(2), n/a-n/a, doi:10.1029/2004GB002254, 2005.

Remaud, M., Chevallier, F., Cozic, A., Lin, X. and Bousquet, P.: On the impact of recent developments of the LMDz atmospheric general circulation model on the simulation of CO_2 transport, Geosci. Model Dev., doi:10.5194/gmd-11-4489-2018, 2018.

Sadok, W. and Jagadish, S. V. K.: The Hidden Costs of Nighttime Warming on Yields, Trends Plant Sci., 25(7), 644–651, doi:10.1016/j.tplants.2020.02.003, 2020.

Sandoval-Soto, L., Stanimirov, M., von Hobe, M., Schmitt, V., Valdes, J., Wild, A. and Kesselmeier, J.: Global uptake of carbonyl sulfide (COS) by terrestrial vegetation: Estimates corrected by deposition velocities normalized to the uptake of carbon dioxide (CO_2), Biogeosciences Discuss., 2(1), 183–201, doi:10.5194/bgd-2-183-2005, 2005.

Seibt, U., Kesselmeier, J., Sandoval-Soto, L., Kuhn, U. and Berry, J. A.: A kinetic analysis of leaf uptake of COS and its relation to transpiration, photosynthesis and carbon isotope fractionation, Biogeosciences, 7(1), 333–341, doi:10.5194/bg-7-333-2010, 2010.

Serio, C., Masiello, G., Mastro, P., Cersosimo, A., Pasquariello, P. and Venafra, S.: Simultaneous retrieval of OCS, and CO2 from the IASI shortwave spectral band: assessment of the accuracy of the retrieval products and validation with in situ observations., in Remote Sensing of Clouds and the Atmosphere XXV, vol. 11531, edited by A. Comerón, E. I. Kassianov, K. Schäfer, R. H. Picard, K. Weber, and U. N. Singh, p. 5, SPIE., 2020.

Stinecipher, J. R., Cameron-Smith, P. J., Blake, N. J., Kuai, L., Lejeune, B., Mahieu, E., Simpson, I. J. and Campbell, J. E.: Biomass Burning Unlikely to Account for Missing Source of Carbonyl Sulfide, Geophys. Res. Lett., 46(24), 14912–14920, doi:10.1029/2019GL085567, 2019.

Stimler, K., Berry, J. A., Montzka, S. A. and Yakir, D.: Association between carbonyl sulfide uptake and 18Δ during gas exchange in C 3 and C 4 leaves, Plant Physiol., 157(1), 509–517, doi:10.1104/pp.111.176578, 2011.

Stimler, K., Montzka, S. A., Berry, J. A., Rudich, Y. and Yakir, D.: Relationships between carbonyl sulfide (COS) and CO_2 during leaf gas exchange, New Phytol., 186(4), 869–878, doi:10.1111/j.1469-8137.2010.03218.x, 2010.

Sun, W., Kooijmans, L. M. J., Maseyk, K., Chen, H., Mammarella, I., Vesala, T., Levula, J., Keskinen, H. and Seibt, U.: Soil fluxes of carbonyl sulfide (COS), carbon monoxide, and carbon dioxide in a boreal forest in southern Finland, Atmos. Chem. Phys., 18(2), 1363–1378, doi:10.5194/acp-18-1363-2018, 2018a.

Sun, W., Maseyk, K., Lett, C. and Seibt, U.: Stomatal control of leaf fluxes of carbonyl sulfide and CO_2 in a Typha freshwater marsh, Biogeosciences, 15(11), 3277–3291, doi:10.5194/bg-15-3277-2018, 2018b.

Sun, W., Maseyk, K., Lett, C. and Seibt, U.: A soil diffusion-reaction model for surface COS flux: COSSM v1, Geosci. Model Dev., 8(10), 3055–3070, doi:10.5194/gmd-8-3055-2015, 2015.

Suntharalingam, P., Kettle, A. J., Montzka, S. M. and Jacob, D. J.: Global 3-D model analysis of the seasonal cycle of atmospheric carbonyl sulfide: Implications for terrestrial vegetation uptake, Geophys. Res. Lett., 35(19), 1–6, doi:10.1029/2008GL034332, 2008.

Tarantola, A.: Inverse problem theory: methods for data fitting and model parameter estimation, Elsevier, Amsterdam, 1987.

Thoning, K. W., Tans, P. P. and Komhyr, W. D.: Atmospheric carbon dioxide at Mauna Loa Observatory. 2. Analysis of the NOAA GMCC data, 1974-1985, J. Geophys. Res., doi:10.1029/JD094iD06p08549, 1989.

Whelan, M. E., Anderegg, L. D. L., Badgley, G., Campbell, J. E., Commane, R., Frankenberg, C., Hilton, T. W., Kuai, L., Parazoo, N., Shiga, Y., Wang, Y. and Worden, J.: Two Scientific Communities Striving for a Common Cause: innovations in carbon cycle science, Bull. Am. Meteorol. Soc., doi:10.1175/bams-d-19-0306.1, 2020.

Whelan, M. E., Min, D. H. and Rhew, R. C.: Salt marsh vegetation as a carbonyl sulfide (COS) source to the
1095   atmosphere, Atmos. Environ., doi:10.1016/j.atmosenv.2013.02.048, 2013.

Whelan, M. E., Hilton, T. W., Berry, J. A., Berkelhammer, M., Desai, A. R. and Elliott Campbell, J.: Carbonyl
        sulfide exchange in soils for better estimates of ecosystem carbon uptake, Atmos. Chem. Phys., 16(6),
        3711–3726, doi:10.5194/acp-16-3711-2016, 2016.

Whelan, M. E., Lennartz, S. T., Gimeno, T. E., Wehr, R., Wohlfahrt, G., Wang, Y., Kooijmans, L. M. J., Hilton,
1100   T. W., Belviso, S., Peylin, P., Commane, R., Sun, W., Chen, H., Kuai, L., Mammarella, I., Maseyk, K.,
        Berkelhammer, M., Li, K. F., Yakir, D., Zumkehr, A., Katayama, Y., Oge, J., Spielmann, F. M., Kitz,
        F., Rastogi, B., Kesselmeier, J., Marshall, J., Erkkila, K. M., Wingate, L., Meredith, L. K., He, W.,
        Bunk, R., Launois, T., Vesala, T., Schmidt, J. A., Fichot, C. G., Seibt, U., Saleska, S., Saltzman, E. S.,
        Montzka, S. A., Berry, J. A. and Elliott Campbell, J.: Reviews and syntheses: Carbonyl sulfide as a
1105   multi-scale tracer for carbon and water cycles., 2018.

Wehr, R., Commane, R., Munger, J. W., Mcmanus, J. B., Nelson, D. D., Zahniser, M. S., Saleska, S. R. and Wofsy,
        S. C.: Dynamics of canopy stomatal conductance , transpiration , and evaporation in a temperate
        deciduous forest, validated by carbonyl sulfide uptake, , 389–401, doi:10.5194/bg-14-389-2017, 2017.

Wei, Y., Liu, S., Huntzinger, D. N., Michalak, A. M., Viovy, N., Post, W. M., Schwalm, C. R., Schaefer, K.,
1110   Jacobson, A. R., Lu, C., Tian, H., Ricciuto, D. M., Cook, R. B., Mao, J. and Shi, X.: The north sulfide
        carbon program multi-scale synthesis and terrestrial model intercomparison project – Part 2:
        Environmental driver data, Geosci. Model Dev., 7(6), 2875–2893, doi:10.5194/gmd-7-2875-2014,
        2014.

Welp, L. R., Keeling, R. F., Meijer, H. A. J., Bollenbacher, A. F., Piper, S. C., Yoshimura, K., Francey, R. J.,
1115   Allison, C. E. and Wahlen, M.: Interannual variability in the oxygen isotopes of atmospheric CO2
        driven by El Niño, Nature, 477(7366), 579–582, doi:10.1038/nature10421, 2011.

Yang, F., Qubaja, R., Tatarinov, F., Rotenberg, E. and Yakir, D.: Assessing canopy performance using carbonyl
        sulfide measurements, Glob. Chang. Biol., 24(8), 3486–3498, doi:10.1111/gcb.14145, 2018.

Yin, X. and Struik, P. C.: C3 and C4 photosynthesis models: An overview from the perspective of crop modelling,
1120   NJAS - Wageningen J. Life Sci., 57(1), 27–38, doi:10.1016/j.njas.2009.07.001, 2009.

Zobler, L.: A World Soil File for Global Climate Modelling. NASA Technical Memorandum 87802, NASA
        Goddard Institute for Space Studies, New York, USA, 1986.

Zumkehr, A., Hilton, T. W., Whelan, M., Smith, S., Kuai, L., Worden, J. and Campbell, J. E.: Global gridded
        anthropogenic emissions inventory of carbonyl sulfide, Atmos. Environ., 183(August 2017), 11–19,
1125   doi:10.1016/j.atmosenv.2018.03.063, 2018.